Supplementary information for:

Anion Controlled Selectivity in Oxygen Reduction Catalysed by a Dinuclear Cobalt N,O-Schiff Base Complex

Charles A. James, Jessica Swindells, Harry Ellis, Richa Arjariya, Samuel P. Jarvis, Adam Brookfield and John Fielden

1. General

Materials and Procedures. Tetrabutylammonium acetate and tetrabutylammonium perchlorate were electrochemical grade and used without further purification. Anhydrous methanol and dimethylformamide (SureSeal) were purchased from Merck. Acetic acid was purchased as analytical grade from Merck. All other materials were purchased as reagent grade from Merck or Fluorochem and used as received.

General Physical Measurements. ^{1}H- and ^{13}C-NMR spectra were acquired using Bruker Ascend 500 (500 MHz) and Bruker Ultrashield Plus 400 (400 mHz) spectrometers. All shifts are quoted with respect to TMS using the solvent signals as secondary standard (s = singlet, d = doublet, t = triplet, q = quartet, p = pentet, dd = doublet of triplets, m = multiplet). Elemental analyses were performed by the University of Manchester Microanalysis laboratory. Mass spectrometry was outsourced to Newcastle University. UV–Vis spectra were obtained with an Agilent Cary 60 UV-Vis spectrophotometer. EPR spectra were acquired at the UK EPSRC National EPR Facility in Manchester, full details are provided in the relevant sections.

2. Synthetic Methods

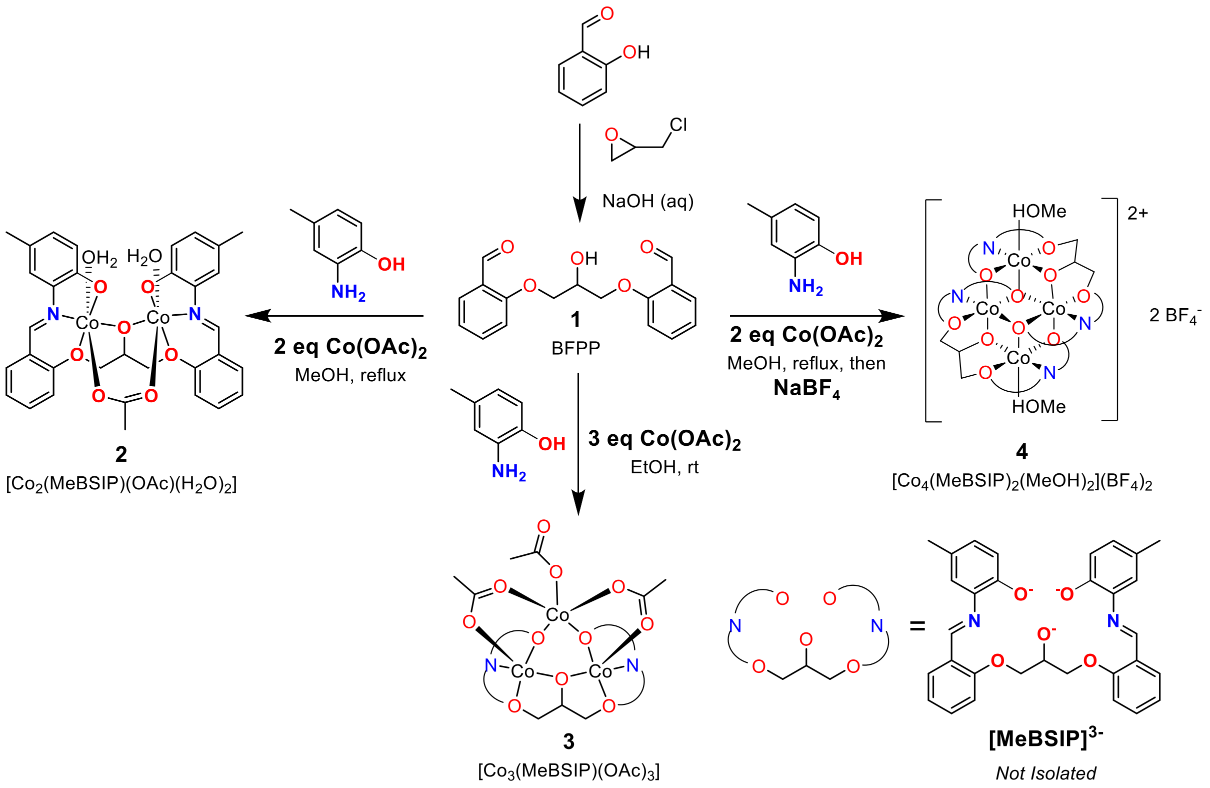

Scheme S1 Overall synthetic approach to compounds **1** to **4**. Conditions reported for **3** are an optimised synthesis, however this compound could also be obtained from reflux in MeOH.

2,2’-[(2-Hydroxy-1,3-propanediyl)bis(oxy)]dibenzaldehyde (BFPP, 1): To a solution of NaOH (9.27 g) in water (250 mL) was added salicylaldehyde (24.0 mL 28.1 g, 230 mmol), the yellow solution was heated to 60 °C under a nitrogen atmosphere before dropwise addition of (±) epichlorohydrin (8.30 mL, 9.8 g, 106 mmol) with vigorous stirring. Heating and stirring were continued for 3 h, then the flask was allowed to cool to room temperature with stirring overnight. After this time, a pale-yellow solid cake formed in the flask. The supernatant was decanted, and the cake was broken up and washed several times with plenty of distilled water. For purification, the solid was dissolved in the minimum amount of hot methanol, cooled to room temperature and then precipitated by slow addition of ice-cold water. The pale-yellow precipitate was washed with water and dried first on the filter then on a high vacuum line (30.1 g, 100 mmol, 43%). ^{1}H-NMR (500 MHz, $CDCl_3$) δ: 10.40 (2 H, s), 7.81 (2 H, dd, *J* = 7.7 Hz, 1.8 Hz), 7.61 – 7.51 (2 H, m), 7.09 (2 H, *t*, *J* = 7.6 Hz, 0.8 Hz), 7.04 (2 H, d, *J* 8.5, 0.9), 4.52 (1 H, p, *J* 5.2), 4.33 (4 H, d, *J* 5.2). ^{13}C-NMR (126 MHz, $CDCl_3$) δ: 189.74, 160.31, 136.11, 130.15, 125.11, 121.53, 113.06, 69.38, 68.39. FTIR (ATR) cm^{-1}: 3456 (m, OH), 1676 (s, C=O).

[Co_2(MeBSIP)(OAc)(H_2O)$_2$] (2): Compound **1** (0.300 g, 1 mmol) and $Co(OAc)_2\cdot 4H_2O$ (0.498 g, 2 mmol) were dissolved in MeOH (30 mL). To the resulting purple solution was added 2-amino-4-methylphenol (0.246 g, 2 mmol), producing an immediate colour change to dark brown. The reaction mixture was stirred at reflux for 3 h before cooling concentrating the solution to 10 mL, then precipitated by dropwise addition of diethyl ether (30 mL). The suspension was filtered, and the precipitate was washed with water (3 × 20 mL) and then diethyl ether (2 × 10 mL). Drying on the filter in air, and then *in vacuo* to yielded **2** as a yellowish brown solid (0.450 g, 0.625 mmol, 63%). *m/z* (ESI$^+$) 625.066 $[(M - OAc - 2\ H_2O)_2]^{2+}$. Anal. for $C_{33}H_{34}Co_2N_2O_9$ calcd (found) %: C 55.01 (55.37), H 4.76 (4.77), N 3.89 (3.83). FTIR (ATR) cm^{-1}: 3250 br (OH, coordinated H_2O), 2927 (w), 2861 (w), 1686 (w), 1599 (s, C=N), 1572 (s, C-O, AcO$^-$ bridging), 1490 (s), 1447 (s), 1417 (s), 1344 (w), 1284 (s), 1244 (s), 1163 (w), 1127 (m), 1105 (sh), 1046 (sh), 1025 (m), 943 (w), 893 (w), 857 (w), 821 (s), 756 (s), 666 (s), 617 (m).

[Co_3(MeBSIP)(OAc)$_3$] (3): Compound **1** (0.300 g, 1 mmol) and cobalt (II) acetate tetrahydrate (0.747 g, 3 mmol) were stirred in ethanol (25 mL) at room temperature for 30 minutes forming a purple suspension. 2-amino-4-methylphenol (0.246 g, 2 mmol) was added to the suspension, resulting in an immediate colour change to dark brown. Over the next 5 minutes of stirring, the suspension dissolved, but after a further hour a brown precipitate began to form. The mixture was stirred for a total of four hours before filtering. The collected solid was washed with cold ethanol (2×10 mL) then diethyl ether (20 mL) and dried in air to yield **3** as a brown solid (0.682 g 0.79 mmol, 79%). *m/z* (MALDI-TOF) 801 $[M - OAc]^+$. Anal. for $C_{37}H_{36}Co_3N_2O_{11}$ calcd (found) %: C 51.58 (51.98), H 4.21 (4.23), N 3.25 (3.25). FTIR (ATR) cm^{-1}: 3200 (br), 2944 (vw), 2922 (w), 2865 (w), 1643 (sh), 1600 (s, C=N), 1576 (s, C-O, AcO$^-$ bridging) 1556 (s, C-O, AcO$^-$ monodentate), 1490 (s), 1443 (s), 1417 (s), 1394 (w), 1382 (w), 1363 (w), 1344 (w), 1321 (w), 1293 (sh), 1283 (m), 1262 (s), 1243 (m), 1221 (m), 1166 (w), 1133 (m), 1093 (w), 1048 (m), 1014 (w), 995 (m), 944 (w), 918 (w), 901 (w), 877 (w), 861 (w), 828 (sh), 819 (s), 793 (w), 760 (vs), 722 (w), 667 (vs), 649 (s), 617 (m), 601 (m).

$[Co_4(MeBSIP)_2(MeOH)_2](BF_4)_2$ (4): To a refluxing solution of **1** (0.301 g, 1 mmol) and cobalt acetate tetrahydrate (0.498 g, 2 mmol) in methanol (25 mL) was added a solution of 2-amino-4-methylphenol (0.246 mg, 2 mmol) in methanol (10 mL). After refluxing for two hours, a solution of $NaBF_4$ (0.109 g, 1 mmol) in methanol (20 mL) was added dropwise without stirring. The solution was allowed to cool and after *ca.* 2 h dark-brown cubic crystals began to form. The crystals were filtered from the supernatant and washed with MeOH (2 × 10 mL) then water (2 × 10 mL) and dried in air overnight to yield crystalline, dark brown **3** (1.20 g, 0.76 mmol, 76%). Anal. for $C_{64}H_{72}B_2Co_4F_8N_4O_{17}$ (**4**•$5H_2O$) calcd (found) %: C 48.59 (48.64), H 4.34 (4.28), N 3.66 (3.67). FTIR (ATR) cm^{-1}: 3608 (w), 3517 (w), 3220 (w, br), 3053 (w), 3024 (w), 1621 (w), 2940 (w), 2878 (w), 1600 (s, C=N), 1575 (w), 1489 (vs), 1457 (vw), 1447 (m), 1417 (vw), 1398 (w), 1385 (w), 1375 (w), 1347 (w), 1260 (s), 1243 (sh), 1234 (sh), 1206 (s), 1177 (w), 1120 (s), 1106 (w), 1060 (vs), 1035 (vs), 1002 (vs), 972 (m), 948 (m), 935 (m), 912 (w), 899 (w), 885 (m), 867 (w), 831 (s), 788 (m), 759 (vs), 694 (m), 655 (w), 612 (w).

2. IR Spectra of 2 to 4

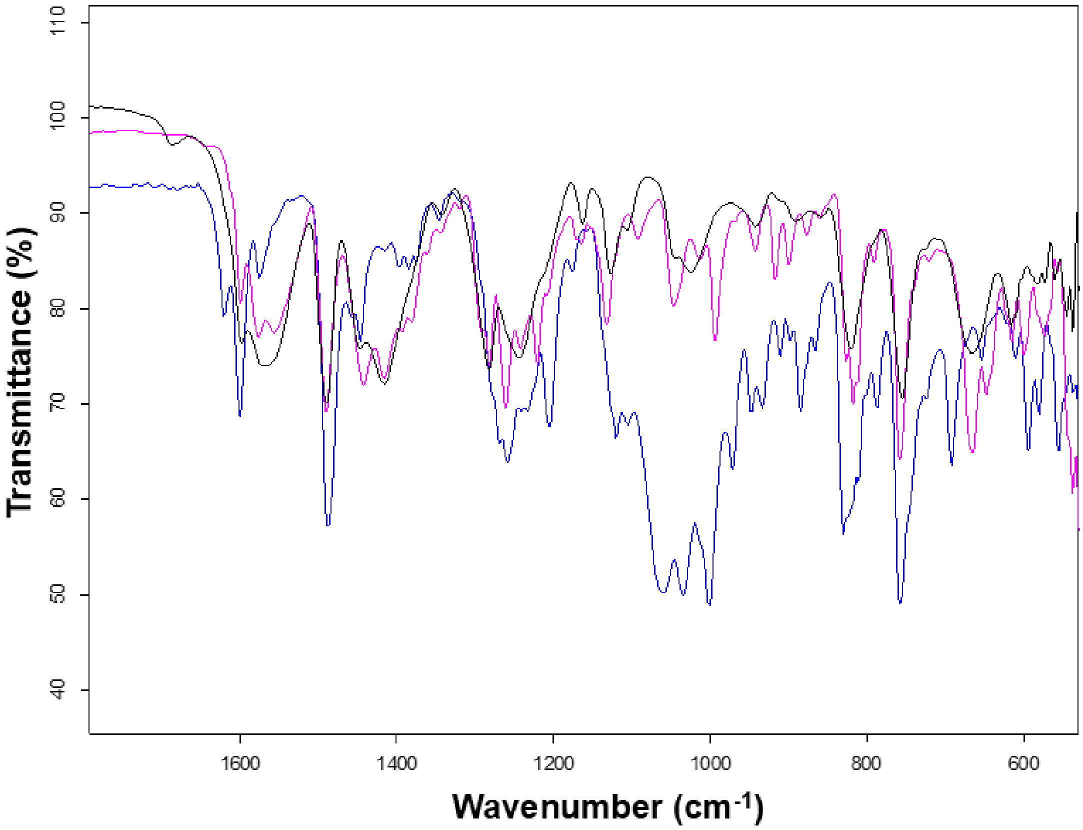

Fig. S1 FTIR spectra of **2** (black), **3** (pink) and **4** (blue) in the range of 1800 to 600 cm^{-1}. Strong absorptions in the 1580 – 1550 cm^{-1} ranges for **2** and **3** are consistent with presence of coordinated acetate, notably for **3** this splits into two clear peaks at 1576 (bridging) and 1558 cm^{-1} (monodentate) while for **2** a broader peak with maximum intensity at 1572 cm^{-1} is observed, assigned to bridging acetate.

3. X-ray Crystallographic Details

Sample Growth, Data Collection and Refinement. X-ray quality crystals of [**3**]•1.5MeOH were grown by slow evaporation of methanol, suitable crystals of [**4**]•4MeOH were isolated from the initial synthesis in methanol. Data were collected on a Rigaku XtalLab Synergy S diffractometer using a Photon-Jet Cu microfocus source and Hypix hybrid photon counting detector. Data reduction, cell refinement and absorption correction were carried out using Rigaku CrysAlisPro,[1] and the structure was solved with SHELXT[2] in Olex2 V1.5.[3] Refinement was achieved by full-matrix least-squares on all F_0^2 data using SHELXL (v. 2019-3),[4] also in Olex 2 V1.5. Crystal data, data collection and refinement parameters are presented in Table S1. The asymmetric unit of [**3**]•1.5MeOH contains one whole [**3**] complex, and one fully occupied and one 50% occupied MeOH solvent (Fig. S1). Disordered electron density resulting from crystal water refined poorly, and was treated using the SQUEEZE routine[5] – this removed 26 electrons from a volume of 124 Å^3 in 2 voids per unit cell, consistent with 1.25 H_2O per formula unit. The asymmetric unit of [**4**]•4MeOH contains the complete **4** complex, four MeOH solvent and both BF_4^- anions, one of these showing positional disorder. Cif files are available from the CCDC, deposition numbers 2447929 (**3**) and 2447930 (**4**).

Table S1. Crystallographic Data and Refinement Details for [**3**]•1.5MeOH and [**4**]•4MeOH

	[3]•1.5MeOH	**[4]•4MeOH**
Formula	$C_{39.5}H_{46}Co_3N_2O_{13.5}$	$C_{68}H_{76}B_2Co_4F_8N_4O_{16}$
M	941.57	1614.66
T/K	100.0(1)	100.1(1)
Crystal system	triclinic	triclinic
Space group	*P*-1	*P*-1
a/Å	11.5896(4)	12.7253(2)
b/Å	13.2720(5)	13.2722(2)
c/Å	14.6041(4)	22.5229(4)
α/°	102.365(3)	97.2080(10)
β/°	105.032(3)	97.696(2)
γ/°	93.290(3)	108.398(2)
V/Å^3	2103.93(13)	3519.64(11)
Z	2	2
ρ_{calc} / g cm-3	1.486	1.524
μ/mm^{-1}	9.718	1.017
Cryst. size/mm^3	0.15 × 0.15 × 0.015	0.31 × 0.27 × 0.25
Cryst. description	Brown plate	Brown block
Radiation	Cu Kα (λ = 1.54184)	MoKα (λ = 0.71073)
2Θ range for data collection/°	6.452 to 158.382	3.71 to 62.138
Reflections collected	24333	57745
Independent reflections (R_{int})	8246 [R_{int} = 0.0790, R_{sigma} = 0.0700]	18079 [R_{int} = 0.0449, R_{sigma} = 0.0472]
Completeness at θ_{full}	97.1%	100%
Data/restraints/parameters	8246/3/545	18079/18/957
Goodness-of-fit on F^2	1.078	1.04
final R_1, wR_2 [I > 2σ(*I*)]	R_1 = 0.0783, wR_2 = 0.2144	R_1 = 0.0486, wR_2 = 0.1283
(all data)	R_1 = 0.0915, wR_2 = 0.2296	R_1 = 0.0681, wR_2 = 0.1377
Peak and hole/e Å^{-3}	1.43/-1.22	1.56/-0.54

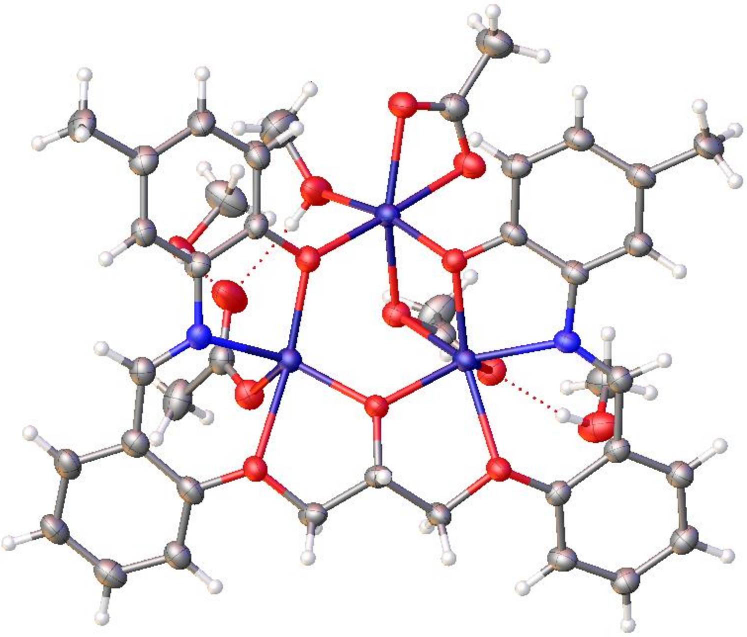

Fig. S2 ORTEP representation of the asymmetric unit in [**3**]•1.5MeOH   Thermal ellipsoids are at the 50% probability level. Colour scheme: Mo is purple; O, red; C, gray; N, blue; H atoms are represented by white spheres of arbitrary radii.

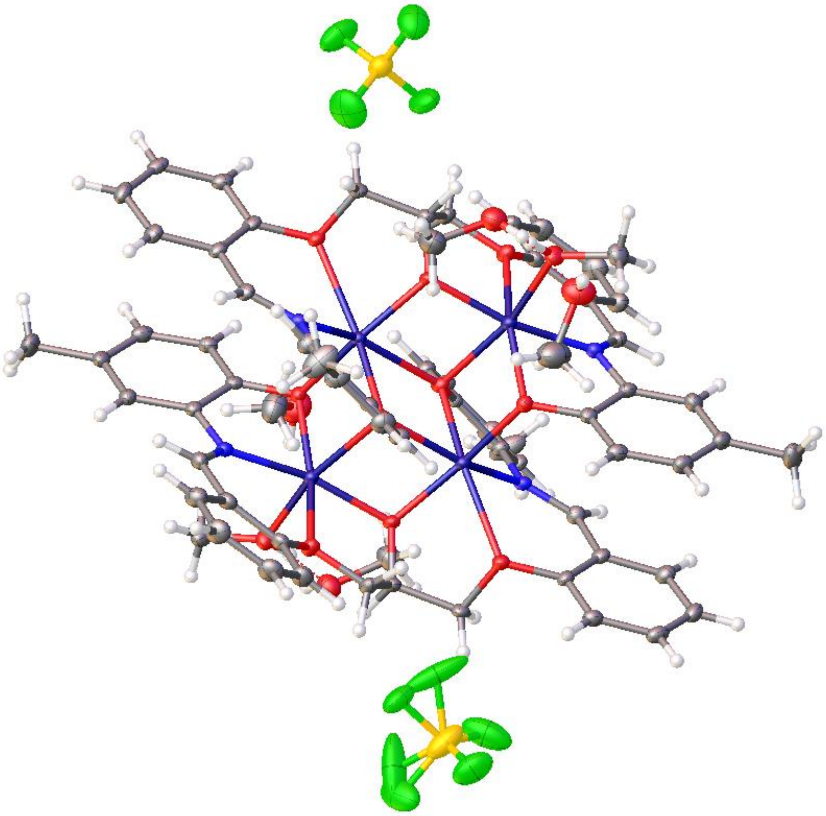

Fig. S3 ORTEP representation of the asymmetric unit in [**4**]•4MeOH   Thermal ellipsoids are at the 50% probability level. Colour scheme: Mo is purple; O, red; C, gray; N, blue; H atoms are represented by white spheres of arbitrary radii.

4. X-ray Photoelectron Spectroscopy (XPS)

Experimental Details. X-ray photoelectron spectra were obtained using a Kratos Analytical AXIS Supra spectrometer with a monochromatic AI Kα 1486.7 eV X-ray source, operating at 15 kV, 15 mA, at vacuum pressures better than 5×10^{-10} mbar, and equipped with an electron gun for charge neutralization. All the spectra were analysed using CASAXPS (Casa Software Ltd, UK).

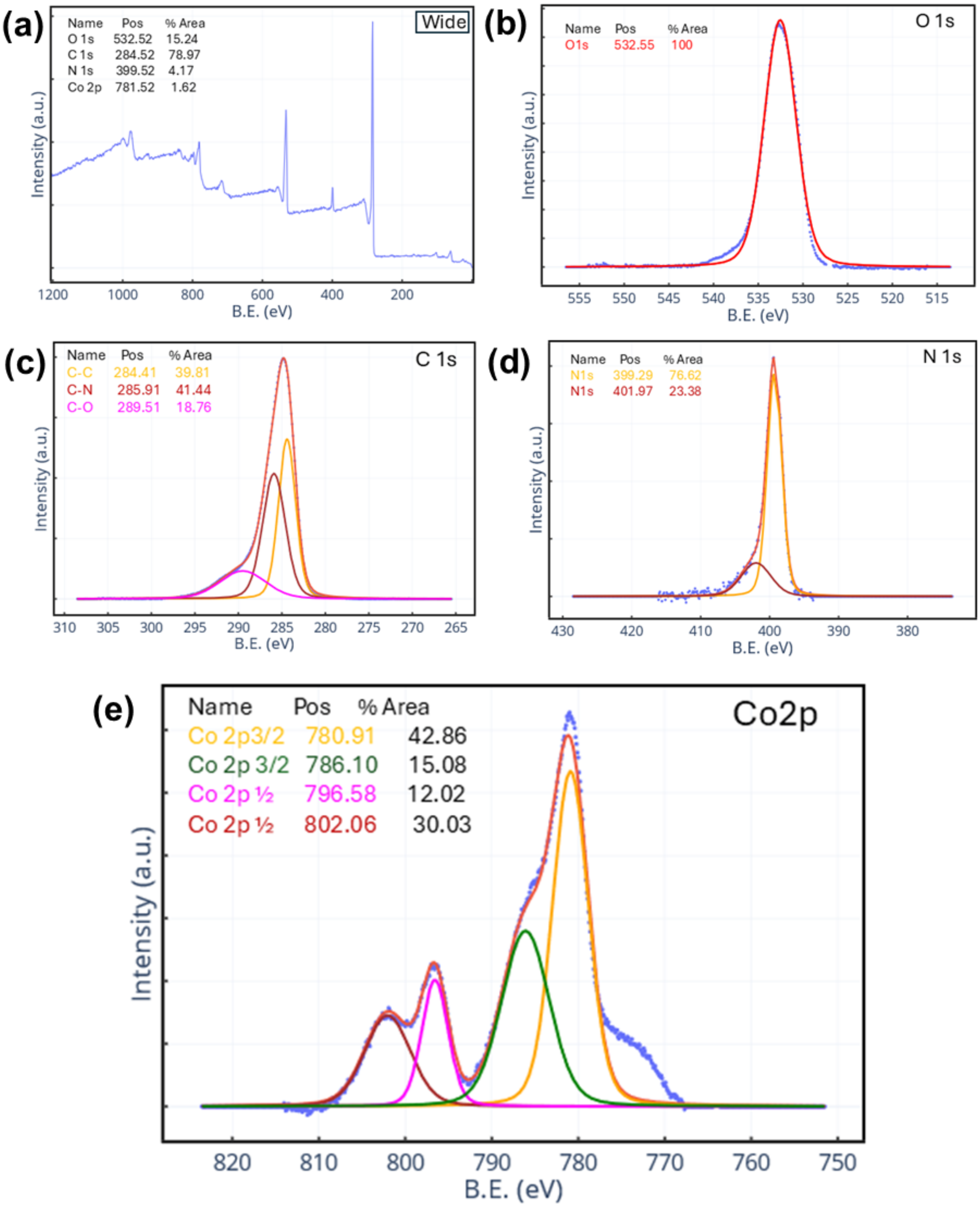

Fig. S4 XPS spectra of solid **2** **(a)** Wide scan showing C, O, N and Co peaks. **(b)** O 1s. **(c)** C 1s. **(d)** N 1s. **(e)** Co 2p. The strong satellites at *ca.* 802 and 786 eV are indicative of Co(II). Presence of Co(III) cannot be excluded, but there are no peaks indicating presence of other Co oxidation states.

Fig. S4 shows overview and region (O 1s, C 1s, N 1s, Co 2p) spectra confirming pure molecular powder free of contamination. As shown in high resolution XPS measured in the Co 2p region in Fig. S4 (e), the absence of a peak around 778 eV in the Co 2p3/2 region, which is characteristic of Co(0), confirms that metallic cobalt is not present. Instead, the spectra show peaks in the expected range for Co^{2+} (typically ~781 eV)[6] and Co^{3+} (typically ~779.5–781 eV),[6,7] along with shake-up satellite[8] features at 5-6 eV that further support the presence of oxidized cobalt species. The strong satellite peaks at 786.56 and 802.07 eV confirm presence of Co^{2+},[8] however the similar ranges expected for Co^{2+} and Co^{3+} main peaks mean that presence of Co^{3+} cannot be excluded.

5. Solid State EPR

Experimental Details. X-band (9.4 GHz) EPR spectra of **2** to **4** at 10 K were obtained using a Bruker EMX X-band spectrometer. Acquisition parameters were 10 scans, 20 dB attenuation and 5G modulation frequency. The spectra are displayed with the frequency corrected to exactly 9.4 GHz in all cases, **2** and **3** have been normalized such that the maximum positive signal is *ca.* 1, the same factor has been applied to **4**. No positive signal is observed for **4** at X-band due to the relatively low frequency. The higher noise level in the spectrum of **2** is due to low sample quantity.

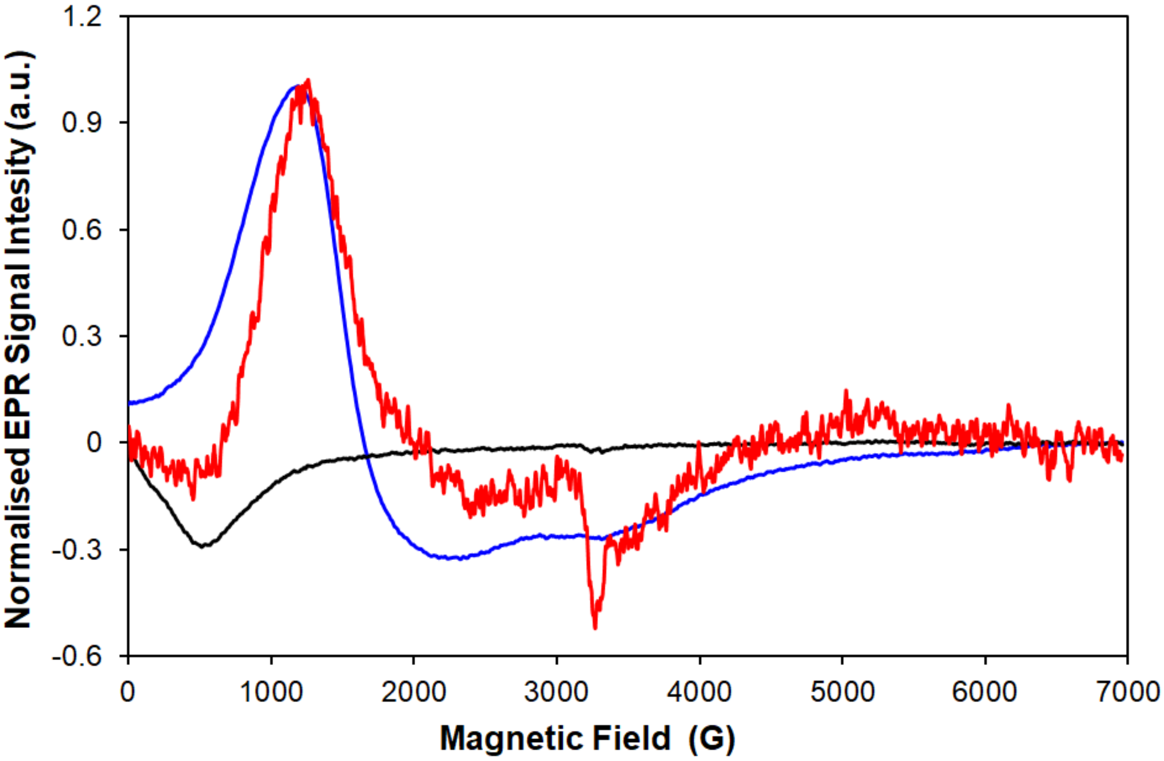

Fig. S5 Solid state X-band EPR spectra of **2** (red), **3** (blue) and **4** (black) obtained at 10 K.

6. Spectrophotometric ORR Activity Assay and TOF Determination

ORR Activity Measurement with Fc* Stoichiometric Reductant. A 0.3 mL air saturated methanolic solution of the complex of interest (200 µM) was added to a quartz UV cuvette along with a 1.7 mL air saturated methanolic solution of Fc* (1.76 mM). A 1 mL air saturated methanolic solution containing 60 mM each AcOH and TBAOAc was rapidly injected into the cuvette before capping and vigorously shaking for 10 seconds, to produce a reaction mixture with initial concentrations: 1 mM Fc*, 20 mM AcOH/TBAOAc, 2 mM O_2 and 20 µM **2**. A UV/Vis trace was then immediately recorded in the range of 900-300 nm and then every 15 seconds thereafter. The ORR was monitored by the growth of the absorbance at 780 nm. Each run was repeated in triplicate to enable estimation of errors.

Data for **2** are presented in the main paper (Fig. 3) and in Fig. S5-S7. Data for **3** and **4**, and a control with no catalyst are shown in Fig.s S8 to S10.

Iodometric Titration to Determine Selectivity. An ORR reaction mixture was allowed to run for 60 minutes to ensure maximum conversion, and 60 µL aliquot was diluted to a 3 mL total volume by addition to MeCN. UV-vis spectra were then acquired before, and 1 h after addition of excess NaI (*ca*. 100 mg) . H_2O_2 present oxidises I^- to produce I_2 which has a strong absorption in the the near UV ($\lambda_{max} = 361$ nm, $\varepsilon = 2.8 \times 10^4$ M^{-1} cm^{-1}). The change in absorbance ΔAbs at 361 nm (Fig. S4) was then used to determine the selectivity for H_2O_2, by predicting the absorbance that would be expected for 100% conversion to H_2O_2:

$$H_2O_2 \text{ selectivity } (\%) = (\Delta Abs_{actual} / \Delta Abs_{theoretical}) \times 100$$

Starting from 1 mM Fc*, a 100% yield of H_2O_2 is 0.5 mM, after 50-fold dilution this gives $\Delta Abs_{theoretical} = 0.28$.

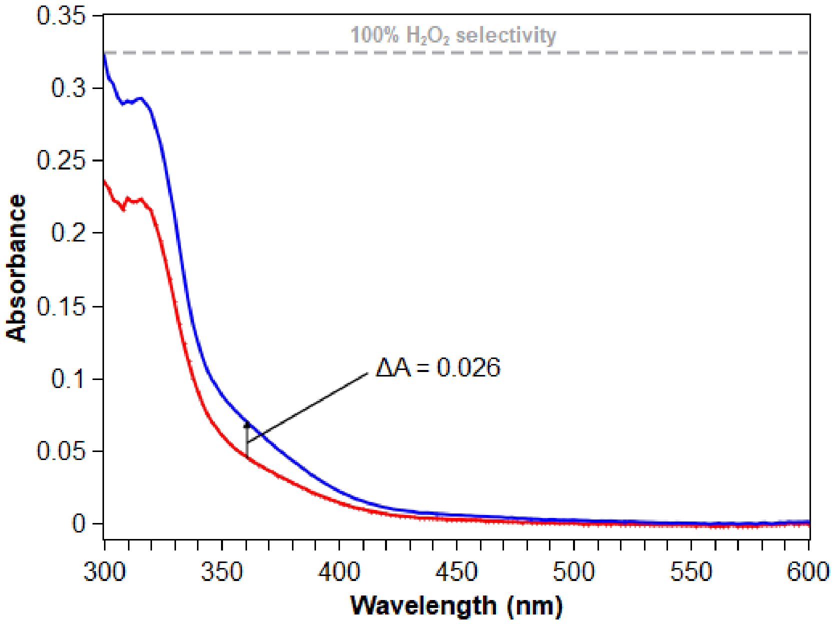

Fig. S6 UV-vis spectrum of a 60 µL aliquot of a complete ORR reaction diluted to 3 mL in MeCN before (red trace) and 1h after (blue trace) addition of excess NaI. The grey dashed line represents the theoretical absorbance value for a catalytic reaction with 100% selectivity for H_2O_2.

This data, for **2** in 20 mM AcOH/TBAOAc, indicates 9.3% selectivity for H_2O_2. As the only other likely product from oxidation of Fc* by air is H_2O, this allows us to estimate a 90.7% selectivity for H_2O.

Note: While it does not directly quantify H_2O or O_2, the approach of using iodometric tirtration to determine H_2O_2, with the rest of the product assigned to O_2 is commonly used and accepted in the literature for chemically driven ORR.[9] This is because there are no oxidants present other than O_2, and H_2O and H_2O_2 are the only possible products. The classic Clark electrode approach to O_2 detection is vulnerable to interference by electroactive species such as Fc*, and using changes in H_2O concentration in hygroscopic solvents such as methanol to determine ORR selectivity is very vulnerable to inaccuracy from exposure to atmospheric moisture.

Estimation of Turnover Frequency. The rate of change in [Fc^{*+}] can be determined from the rate of change in Fc^{*+} absorbance at 780 nm.

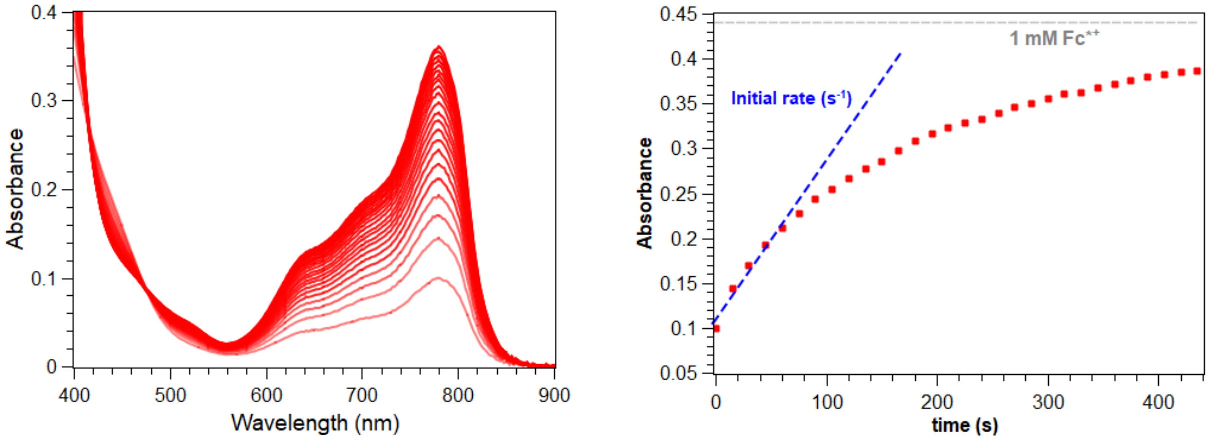

Fig. S7 Left: UV-vis spectra showing increase in 780 nm absorption over time in an ORR run. **Right:** Determination of initial rate of change of absorbance in s^{-1}.

By using the Beer-Lambert Law the rate of change in absorbance can be converted to a rate in change of [Fc^{*+}]

$$\frac{d[Fc^{*+}]}{dt} = \frac{dA_{780}}{dt}\frac{1}{\varepsilon_{780}}$$

In acidic MeOH with no catalyst, very slow oxidation of Fc* to Fc^{*+} is still observed. This has a rate on the order of 10^{-7} M s^{-1} and is subtracted to give the catalytic rate.

$$\frac{d[Fc^{*+}]}{dt}_{catalysed} = \frac{d[Fc^{*+}]}{dt}_{total} - \frac{d[Fc^{*+}]}{dt}_{background}$$

The 90.7% selectivity for H_2O determined above means that 90.7% of the Fc* and thus 90.7% of the electrons are being consumed by the 4 electron pathway to H_2O, 9.3% are being consumed by the 2 electron pathway to H_2O_2. Assuming the selectivity is the same throughout the reaction, this means the initial overall catalysed rate of production of Fc^{*+} of 2.72×10^{-6} M s^{-1} feeds through to 2.467×10^{-6} M s^{-1} for the H_2O process, and 2.530×10^{-7} M s^{-1} for the H_2O_2 process. TOF can be calculated with the following equation:

$$TOF = \frac{\frac{d[Fc^{*+}]}{dt}_{catalysed}}{n * [\boldsymbol{Cat}]}$$

Where n is the number of electrons involved (4 for H_2O, 2 for H_2O_2). This gives:

$TOF_{H2O} = 0.031\ s^{-1}$ (to 2 s.f.)

$TOF_{H2O2} = 0.0063\ s^{-1}$ (to 2 s.f.)

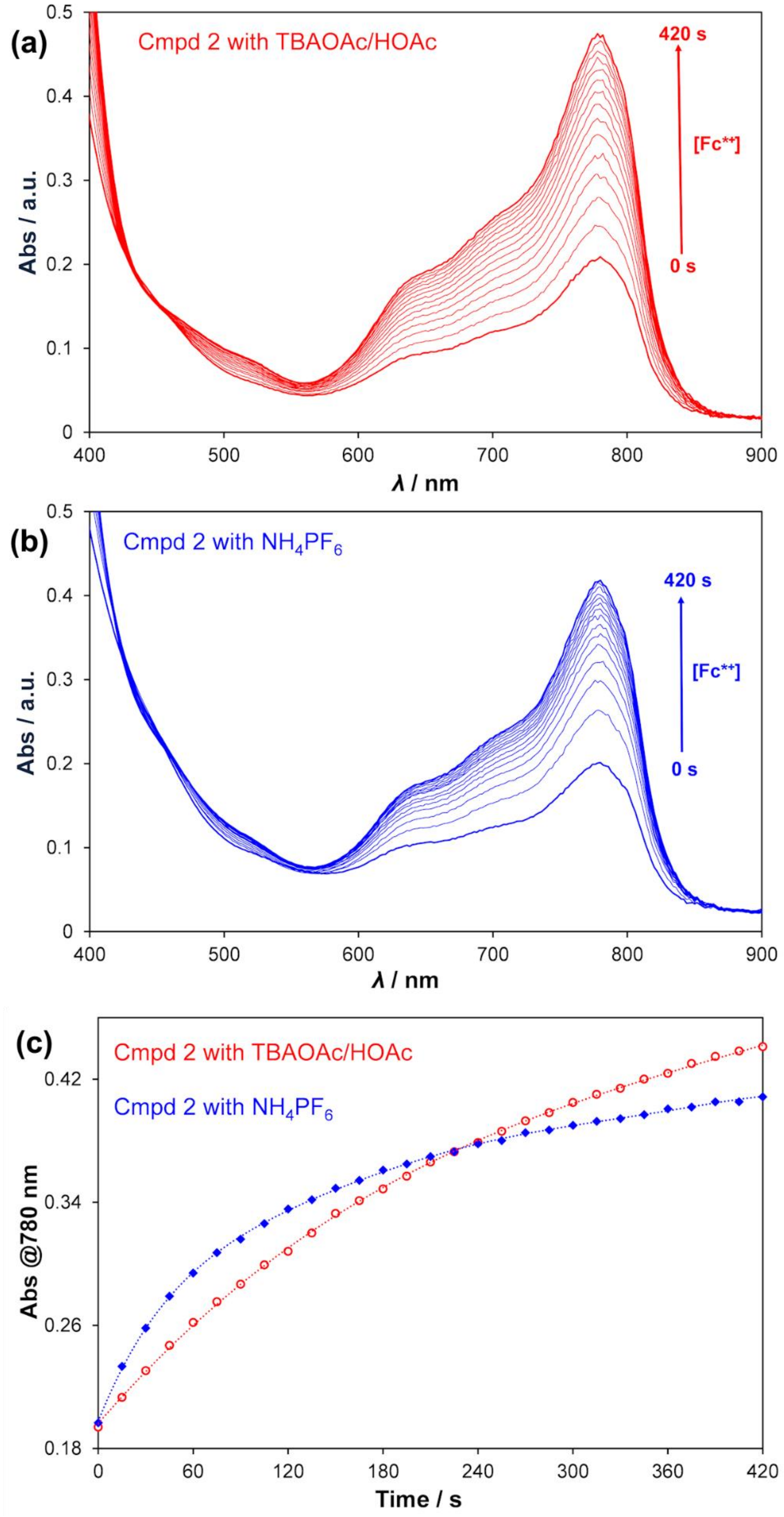

Fig. S8 Evolution of ORR reactions carried out with 20 μM **2**, 1 mM Fc* and 2 mM O_2 in different buffers, monitored by production of Fc^{*+} through absorbance at 780 nm. (**a**) 10 mM HOAc/10 mM NBu_4OAc. (**b**) 10 mM NH_4PF_6. (**c**) Change in absorbance at 780 nm over time in the two conditions, showing faster initial rate in NH_4PF_6 medium.

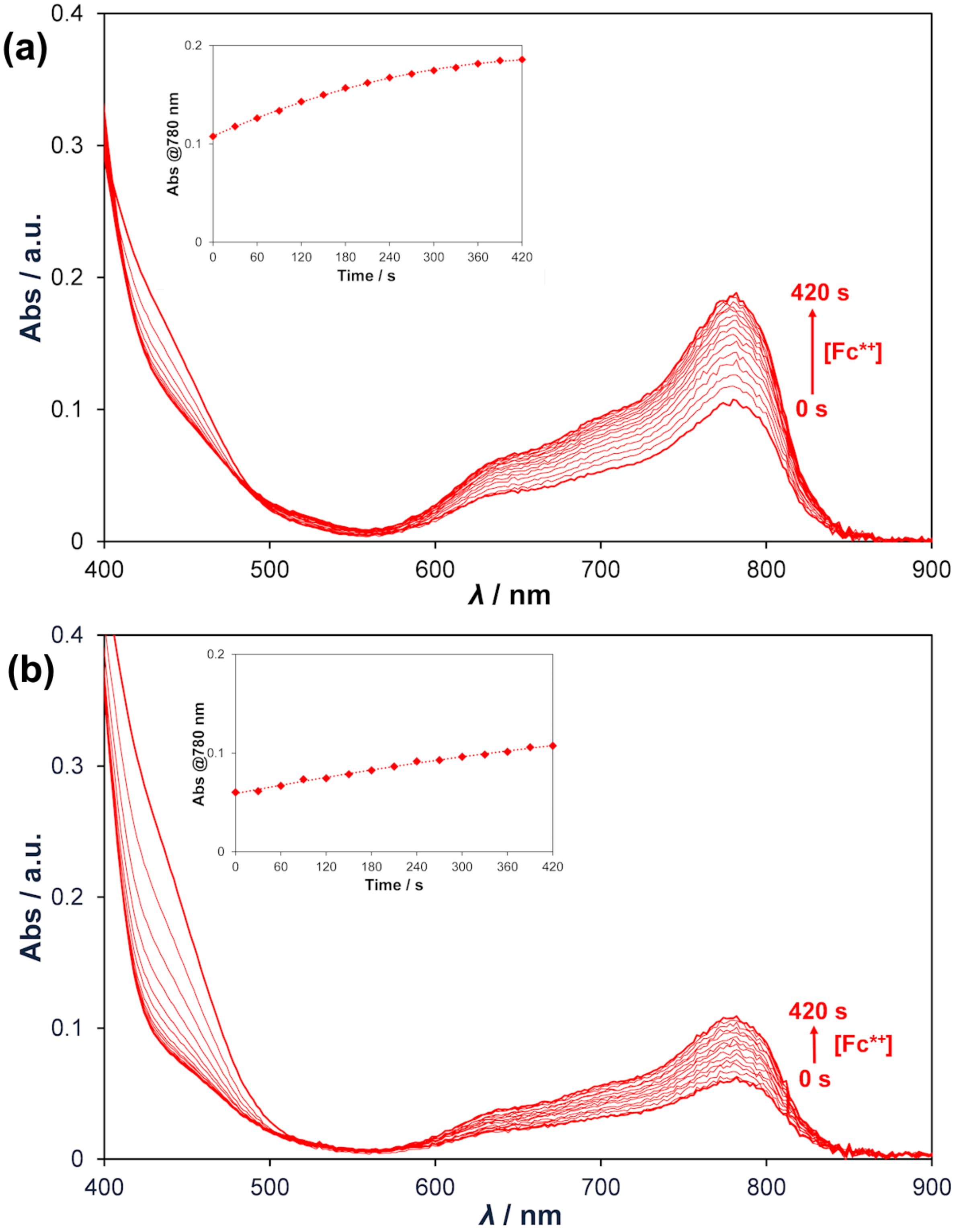

Fig. S9 **(a)** UV-vis spectra showing increase in 780 nm absorption (corresponding to production of Fc^{*+}) over time in an ORR run using compound **3**. **(b)** UV-vis spectra showing increase in 780 nm absorption over time in an ORR run using compound **4**. Insets show change in absorbance at 780 nm vs time for each data set. Conditions: 20 μM complex, 1 mM Fc*, 10 mM HOAc, 10 mM NBu_4OAc, 2 mM O_2.

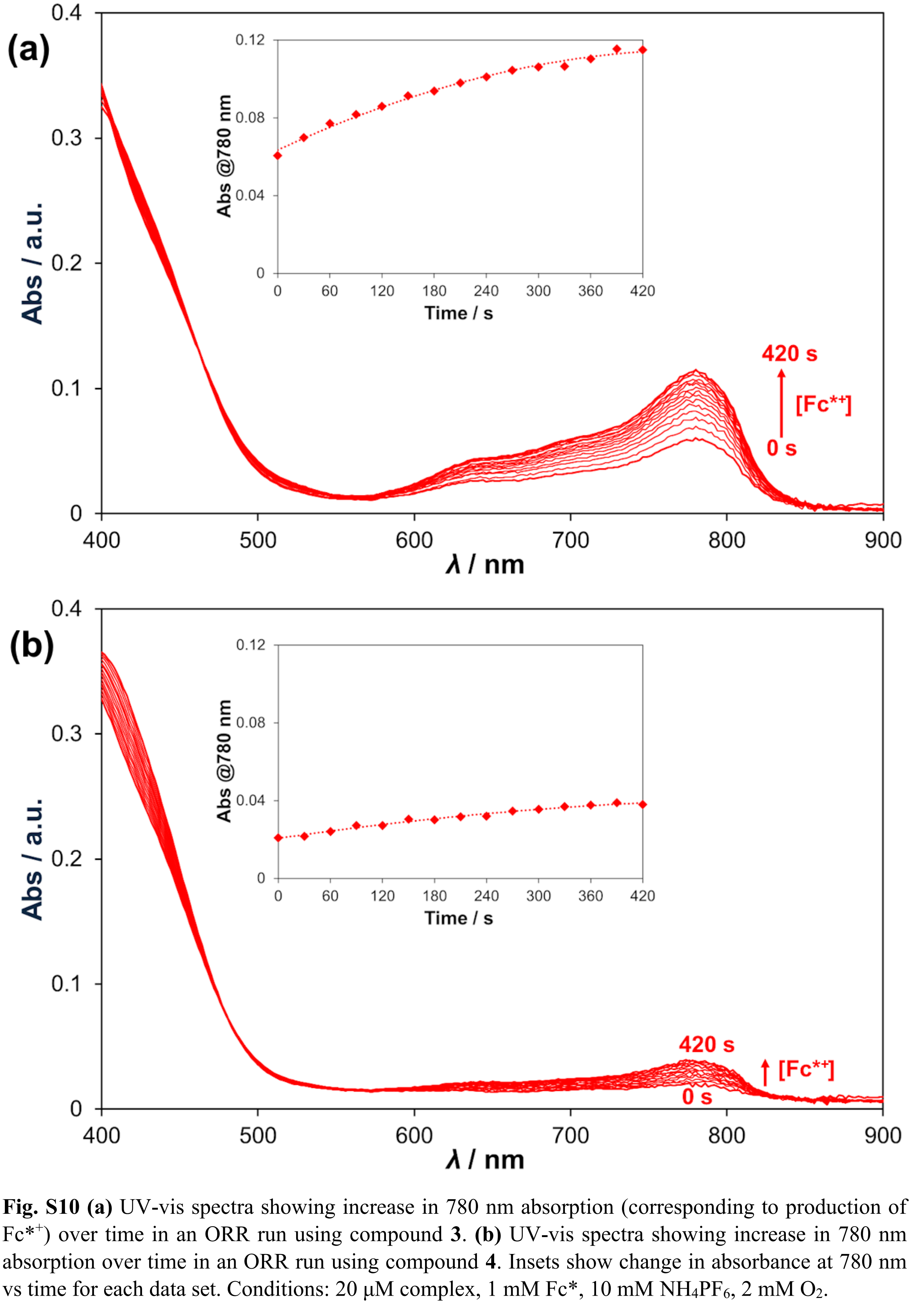

Fig. S10 **(a)** UV-vis spectra showing increase in 780 nm absorption (corresponding to production of Fc^{*+}) over time in an ORR run using compound **3**. **(b)** UV-vis spectra showing increase in 780 nm absorption over time in an ORR run using compound **4**. Insets show change in absorbance at 780 nm vs time for each data set. Conditions: 20 μM complex, 1 mM Fc*, 10 mM NH_4PF_6, 2 mM O_2.

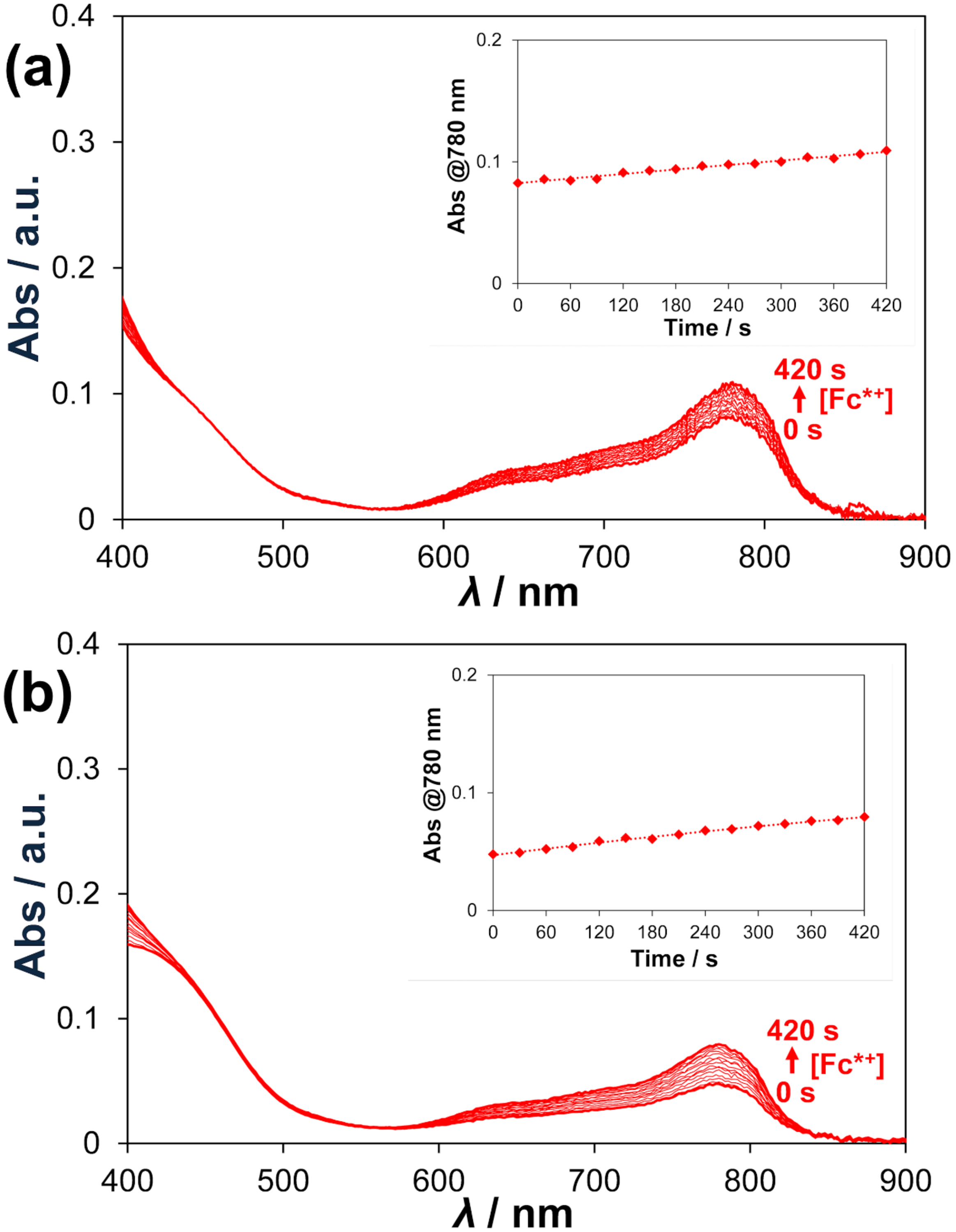

Fig. S11 UV-vis spectra showing increase in 780 nm absorption (corresponding to production of Fc^{*+}) over time in blank ORR runs (no catalyst). Insets show change in absorbance at 780 nm vs time. Conditions: (**a**) 1 mM Fc*, 20 mM HOAc, 20 mM NBu_4OAc, 2 mM O_2 (**b**) 1 mM Fc*, 20 mM NH_4PF_6, 2 mM O_2.

5. Electrochemistry

Cyclic voltammetry (CV). All measurements were carried out using Autolab PGStat 302 or PGStat 30 potentiostats. A single-compartment three-electrode cell was used with an Ag wire pseudo reference electrode, glassy carbon working electrode and Pt wire auxiliary electrode. Electrolytes were 0.1 M $[NBu_4][PF_6]$ in DMF, or 0.05 M $[NBu_4][ClO_4]$ in methanol, and solutions containing *ca.* 10^{-3} M analyte were degassed by purging with argon and blanketed with a continuous flow of argon throughout the experiments. Decamethylferrocene (Fc*) was used as an internal reference following each electrochemical experiment, and all potentials are reported referenced to $Fc^{*0/+}$. $E_{1/2}$ values were calculated from $(E_{pa} + E_{pc})/2$ at a scan rate of 100 mV s^{-1}.

Voltammetry of 2 to 4 in MeOH/$[NBu_4][ClO_4]$. Owing to the poor solubility of **3** and **4** in MeOH, these complexes were first dissolved in the minimum possible amount of dimethylformamide before addition to 0.05 M $[NBu_4][ClO_4]$ in methanol. Electrochemistry in DMF was also attempted but peaks were very poorly resolved in this solvent.

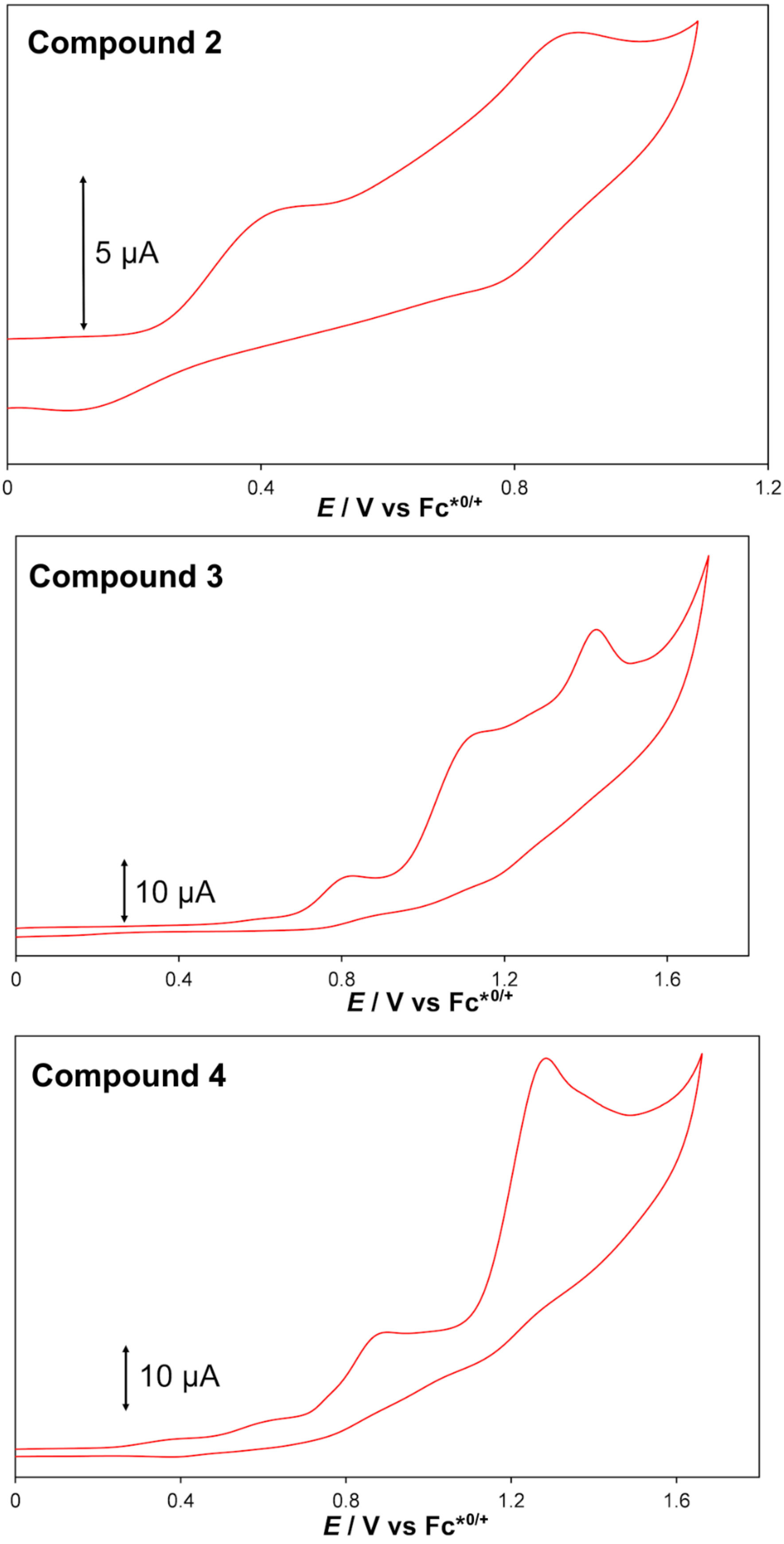

Fig. S12 Cyclic voltammograms of *ca.* 10^{-3} M **2** to **4** in MeOH, supporting electrolyte 0.05 M $[NBu_4][ClO_4]$. Scan rate 100 mV s^{-1}, potentials referenced to $Fc^{*0/+}$.

Cyclic voltammetry of 2 in MeOH with added AcOH. The effect of adding AcOH to **2** in MeOH (0.05 M $[NBu_4][ClO_4]$) is shown in Fig. S12. Emergence of a new wave (2A) is seen at a similar potential to the shift in the second wave in the presence of AcOH/TBAOAc (main paper). This is consistent with assignment to the electrochemically generated anation product [**2**(OAc)] produced after the first oxidation. However, the non-buffered system is not as effective at delivering AcO^- so the original second wave (2B) is still observed. A shift to more positive potential in the first wave occurs (particularly the return part), consistent with protonation of the ligand facilitating reduction of $[\mathbf{2}]^+$ (in fact $[\mathbf{2}H]^{2+}$ or $[\mathbf{2}(HOAc)]^+$) and lowering the overpotential for the ORR.

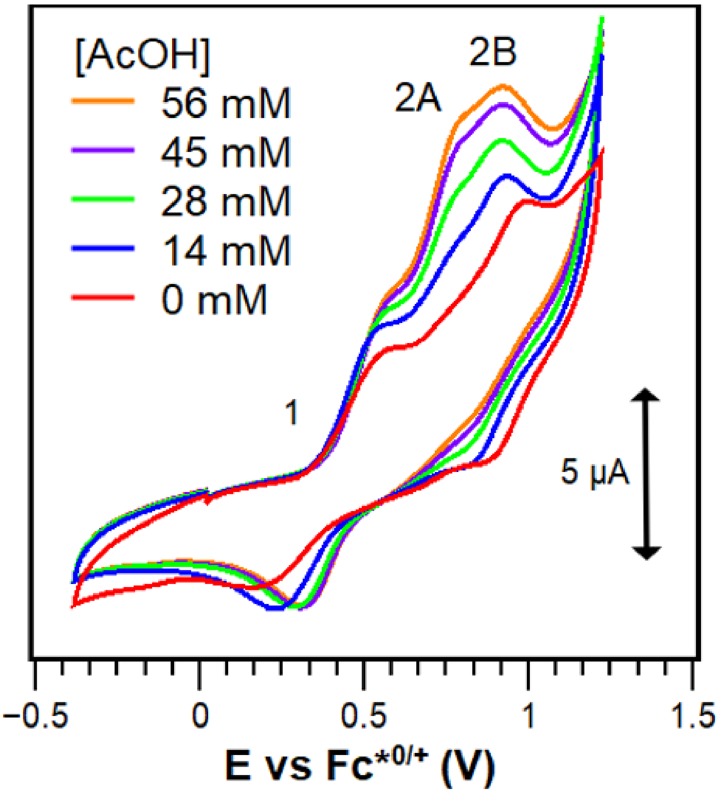

Fig. S13 Cyclic voltammogram of **2** in MeOH, supporting electrolyte 0.05 M $[NBu_4][ClO_4]$, with addition of AcOH. Scan rate 100 mV s^{-1}, potentials referenced to $Fc^{*0/+}$

Cyclic voltammetry of 2 in MeOH with added NH_4PF_6. When NH_4PF_6 is added, instead of the negative shift observed in the AcOH/TBAOAc buffer, a small positive shift is seen in the redox potentials of **2** (Fig. S13). This is ascribed to protonation of **2**, without coordination. The peak at *ca.* +1.2 V is assigned to oxidation to a $Co^{III}Co^{IV}$ species overlapped with destructive ligand oxidation processes.

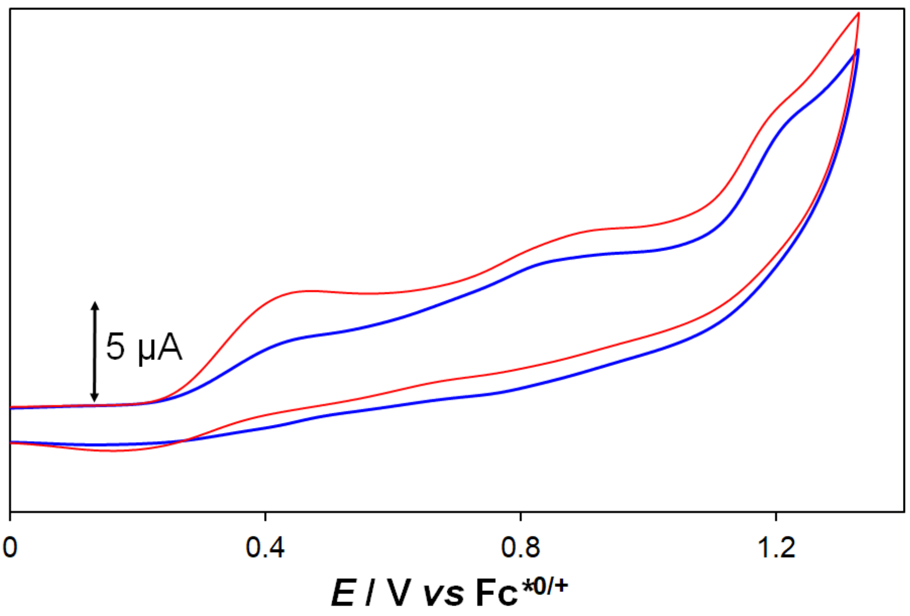

Fig. S14 Cyclic voltammogram of **2** (1 mM) before (blue) and after (red) addition of NH_4PF_6 (25 mM). MeOH, 50 mM $TBAClO_4$, glassy carbon electrode, 100 mV s^{-1}.

Cyclic voltammetry of 2 in MeOH under air saturated conditions. In both the AcOH/TBAOAc and NH_4PF_6 media, saturation of the solution with air produces a positive shift in the $[\mathbf{2}]^{0/+}$ (or $[\mathbf{2}]^{+/2+}$ if AcO^- is decoordinated) redox couple, of 20 to 30 mV. This is indicative of O_2 binding.[9c,10] Separations ΔE also become smaller, consistent with binding of O_2 between the two cobalts making the complex more rigid. Under both conditions the second ($[\mathbf{2}]^{+/2+}$) wave becomes weaker in the presence of O_2. Potentially, this, and the relative lack of a shift in the return wave of the $[\mathbf{2}]^{0/+}$ process, are explained by decoordination of O_2 during the oxidation process.

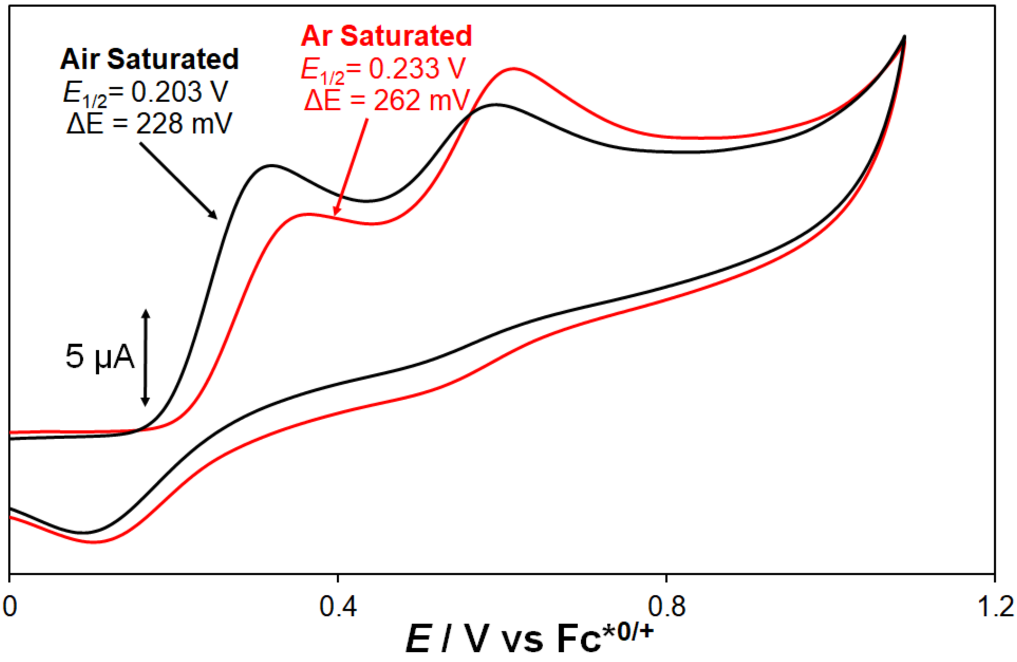

Fig. S15 Cyclic voltammogram of **2** (1 mM) in the presence of AcOH/TBAOAc (25 mM) under argon saturated (red) and air saturated (black) conditions. Electrolyte 50 mM $TBAClO_4$ in MeOH, glassy carbon electrode, 100 mV s^{-1}.

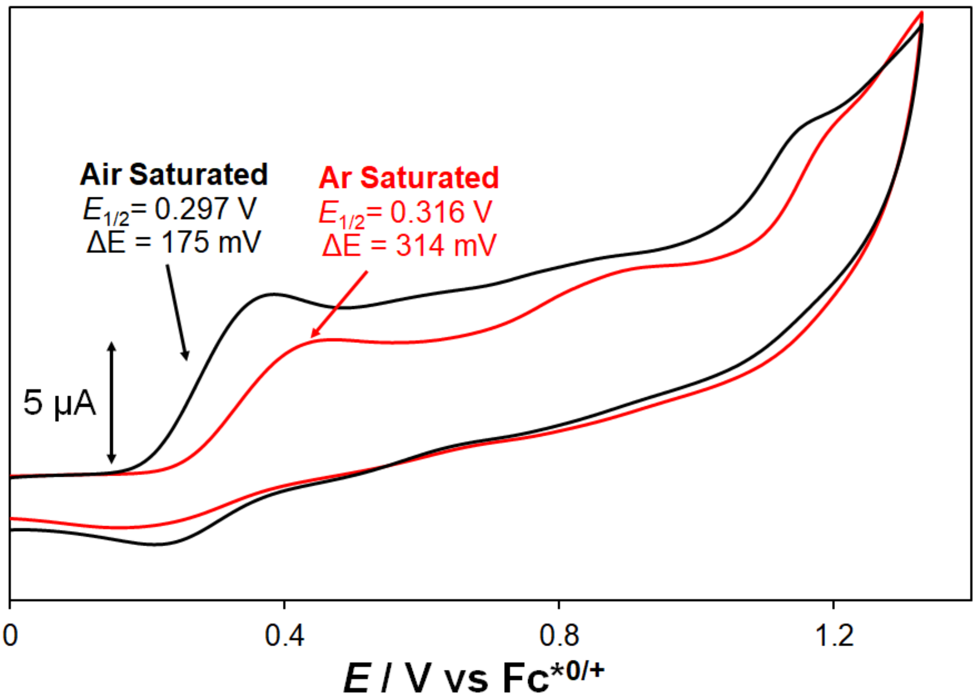

Fig. S16 Cyclic voltammogram of **2** (1 mM) in the presence of NH_4PF_6 (25 mM) under argon saturated (red) and air saturated (black) conditions. Electrolyte 50 mM $TBAClO_4$ in MeOH, glassy carbon electrode, 100 mV s^{-1}.

6. Determination of the catalytic rate law of 4-electron ORR with 2

General method. The general method was as described for the Fc* driven ORR activity assay and TOF determination (section 4). For each variation described below, runs were performed in triplicate to enable estimation of errors.

Variation of [2]. 0.3 mL solutions of **2** were prepared in air saturated MeOH, at concentrations at concentrations between 40 and 400 µM. Dilution to a total volume of 3 mL in the experiments produced initial concentrations of **2** in the reaction mixture in the range of 4 to 40 µM. Initial concentrations of the other components were: 1 mM Fc*, 20 mM AcOH/TBAOAc, 2 mM O_2.

Variation of [Fc*]. Air saturated MeOH containing 0.88 mM Fc* was added to the other reagents to solutions with a total volume of 3 mL MeOH, and [Fc*] of 0.2 to 0.8 mM. Initial concentrations of the other components were: 20 mM AcOH/TBAOAc, 2 mM O_2, 5 µM **2**.

Variation of unbuffered [AcOH]. Air saturated MeOH containing 60 mM AcOH was added in quantities of 0, 0.25, 0.5 or 0.75 mL to the other reagents, to give solutions with a total volume of 3 mL MeOH. This resulted in initial [AcOH] of 5, 10, 15 or 20 mM in the reaction mixtures. Initial concentrations of other components were: 1 mM Fc*, 20 µM **2**, 2 mM O_2.

Variation of [O_2]. Reaction mixtures were prepared as described in section 4 but to achieve approximate starting [O_2] of 9 mM, 6.5 mM and 4 mM, a 2.7 mL, 1.7 mL or 1 mL portion of the 3 mL mixture was saturated with O_2, instead of air before mixing with the rest. For 2 mM, the entire volume was air saturated. Initial concentrations of other components were: 1 mM Fc*, 20 mM AcOH/TBAOAc and 30 µM **2**.

Variation of [AcOH/TBAOAc]. Air saturated MeOH containing 30 mM each of AcOH and TBAOAc was added in quantities of 0.4, 0.8, 1.2 and 1.6 mL to the other reagents, to give solutions with a total volume of 3 mL MeOH. This resulted in initial [AcOH/TBAOAc] of 2, 4, 6, or 8 mM in the reaction mixtures. Concentrations of the other components were retained at: 1 mM Fc*, 20 µM **2**, 2 mM O_2.

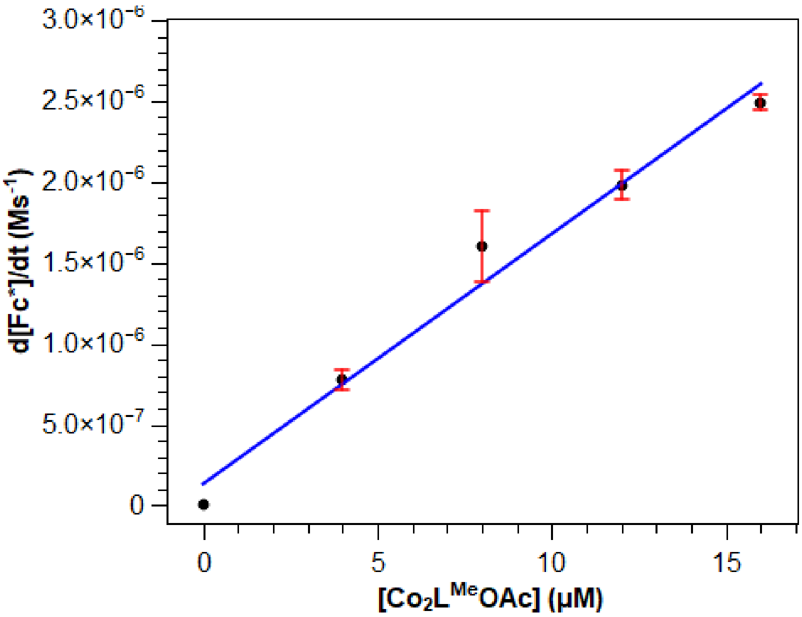

Fig. S17 ORR rate vs [**2**] plot in the presence of AcOH/TBAOAc (20 mM), Fc* (1 mM) and O_2 (2 mM) showing first order dependence on [**2**] at low concentrations.

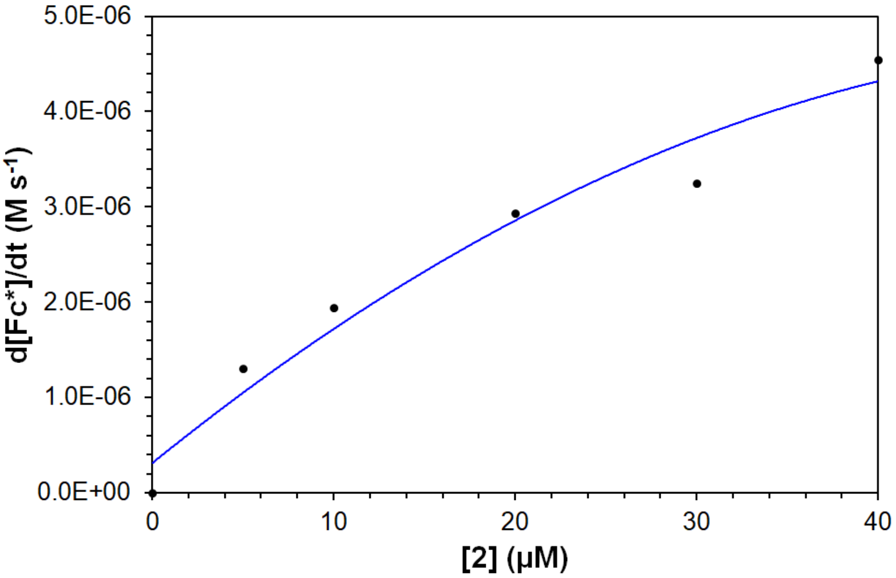

Fig. S18 ORR rate vs [**2**] plot in the presence of AcOH/TBAOAc (20 mM), Fc* (1 mM) and O_2 (2 mM) showing attenuation of first order dependence on [**2**] at higher catalyst concentrations.

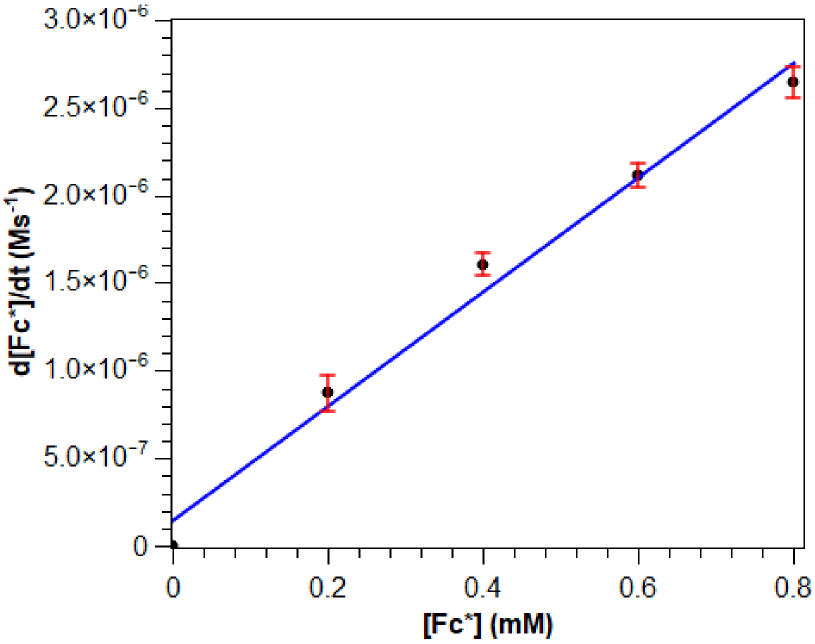

Fig. S19 ORR rate vs [Fc*] plot in the presence of **2** (20 µM), AcOH/TBAOAc (20 mM) and O_2 (2 mM).

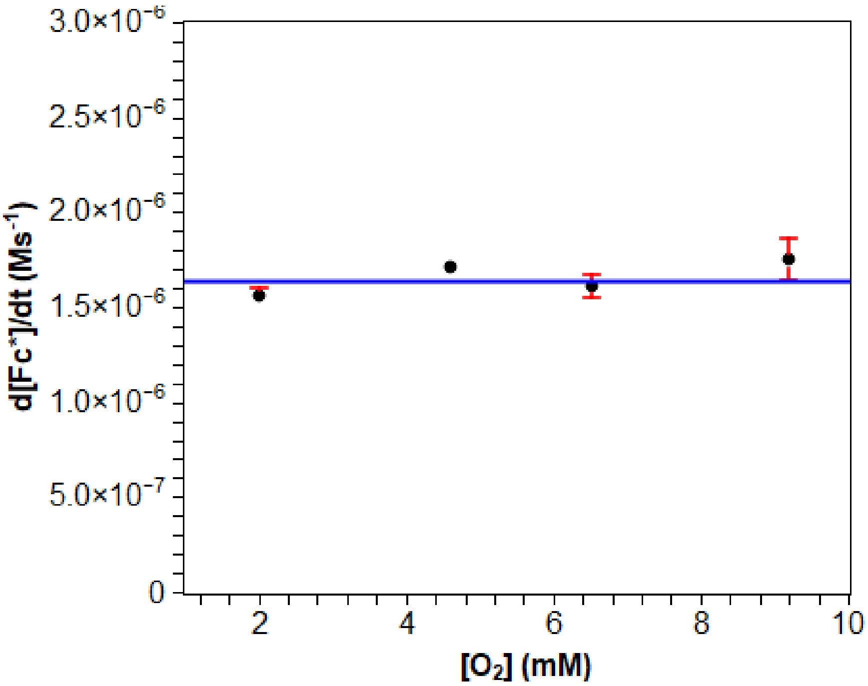

Fig. S20 ORR rate vs [O_2] plot in the presence of **2** (20 µM), Fc* (1 mM) and AcOH/TBAOAc (20 mM).

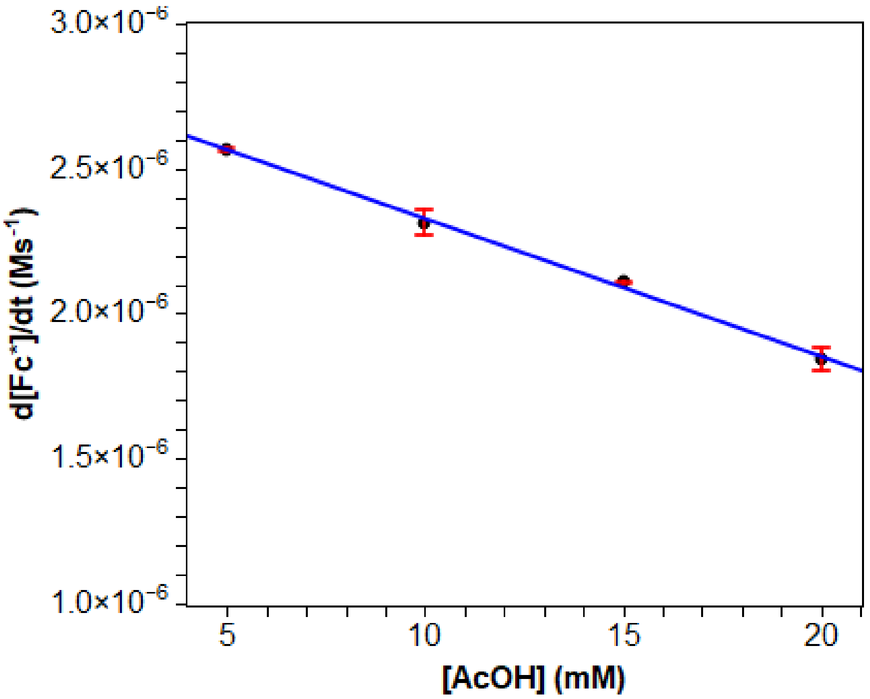

Fig. S21 Unbuffered ORR rate vs [AcOH] plot in the presence of **2** (20 µM), Fc* (1 mM) and O_2 (2 mM).

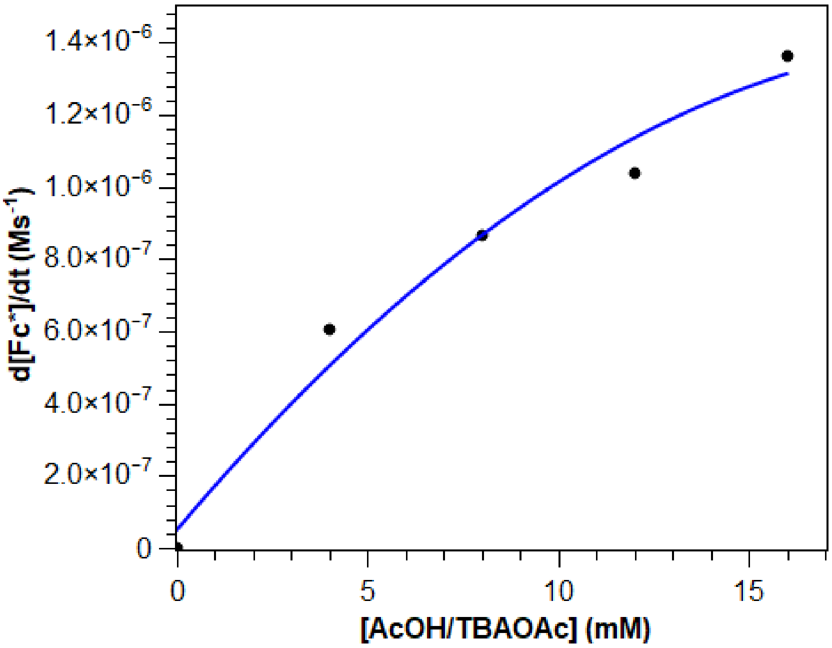

Fig. S22 ORR rate vs [AcOH/TBAOAc] plot in the presence of **2** (20 µM), Fc* (1 mM) and O_2 (2 mM). The rate of background ORR where MeOH is the proton source is significant in these conditions, and is subtracted to give the true effect of AcOH/TBAOAc on rate.

7. Investigation of the kinetics of 2-electron ORR with 2 in the presence of NH_4PF_6

Similar methods were used to those described for AcOH/TBAOAc. Reaction rates show an initially strong dependence on [**2**], [Fc*] and [NH_4PF_6] that attenuates much more rapidly than in the AcOH/TBAOAc buffer. This could be due to lower stability of [**2**] when there is no acetate co-ligand in solution, leading to more off-cycle deactivation pathways. It could also reflect a lower reaction order in catalyst, electrons and protons, consistent with the two electron pathway.

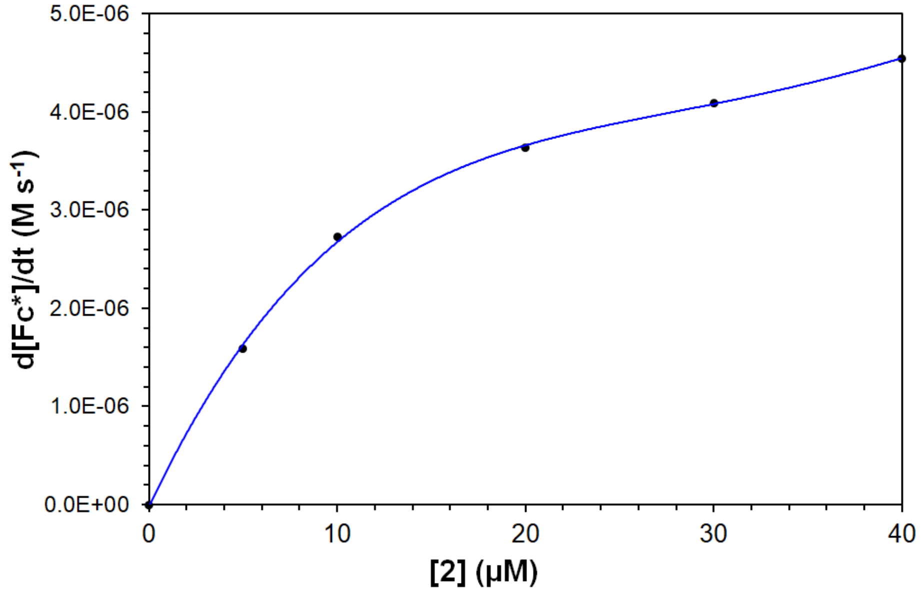

Fig. S23 ORR rate vs [**2**] plot in the presence of NH_4PF_6 (10 mM), Fc* (1 mM) and O_2 (2 mM) showing more rapid attenuation of rate dependence than for AcOH/TBAOAc

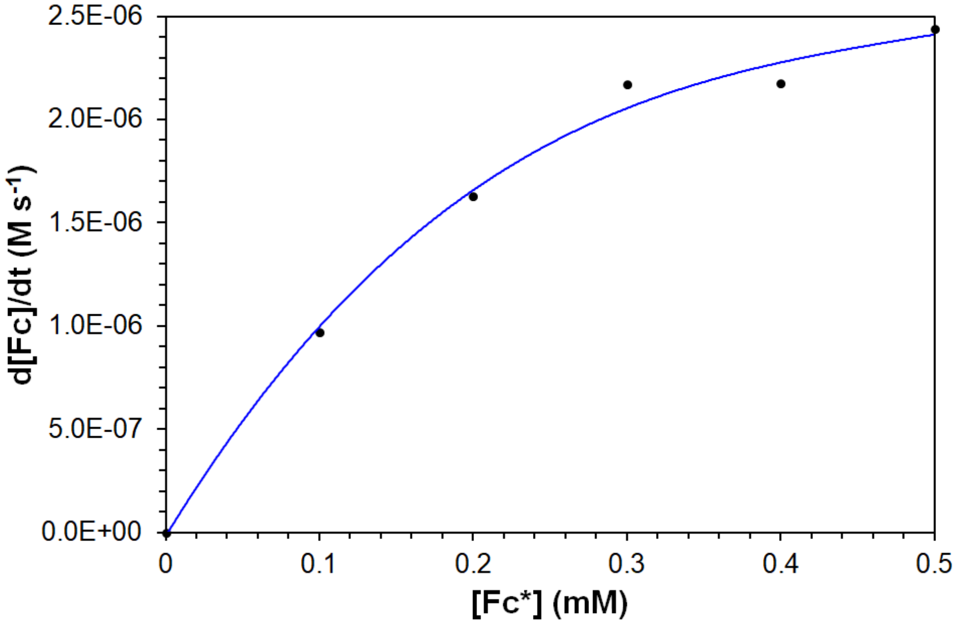

Fig. S24 ORR rate vs [Fc*] plot in the presence of **2** (20 μM), NH_4PF_6 (10 mM) and O_2 (2 mM).

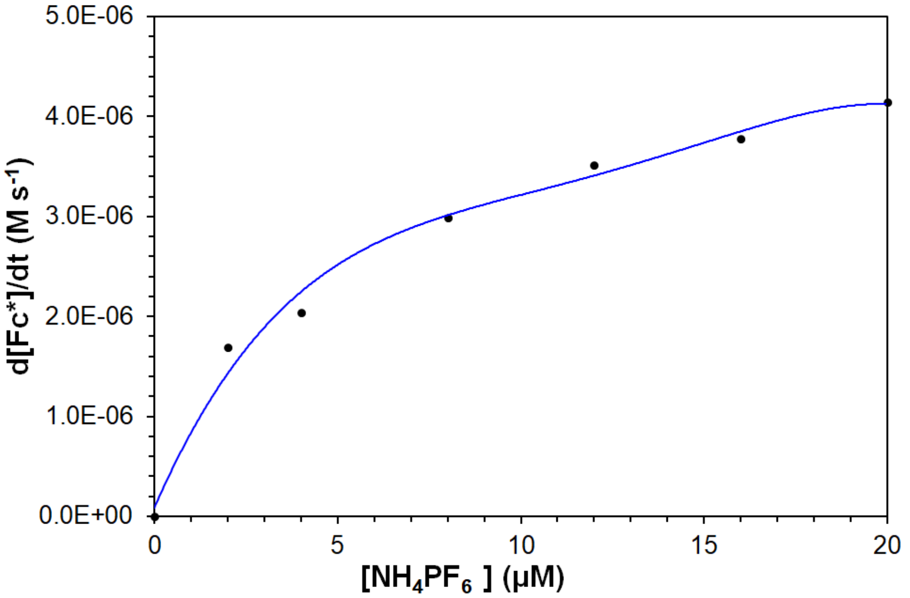

Fig. S25 ORR rate vs [NH_4PF_6] plot in the presence of **2** (20 μM), Fc* (1 mM) and O_2 (2 mM). The rate of background ORR where MeOH is the proton source is significant in these conditions, and is subtracted to give the true effect of [NH_4PF_6] on rate.

8. NMR and EPR spectroscopy of 2 under catalytic conditions

NMR Spectroscopy. The NMR spectrum of **2** in CD_3OD is presented in Fig. S16 (**top**). Broadening, and observation of a number of peaks at high chemical shift is consistent with the paramagnetic, dicobalt(II) complex. The same spectrum is observed both under saturation with air, and with argon. However, after addition of AcOH, paramagnetic shifts disappear, suggesting presence of acetate and H^+ results in binding of O_2 and generation of a diamagnetic dicobalt(III) species.

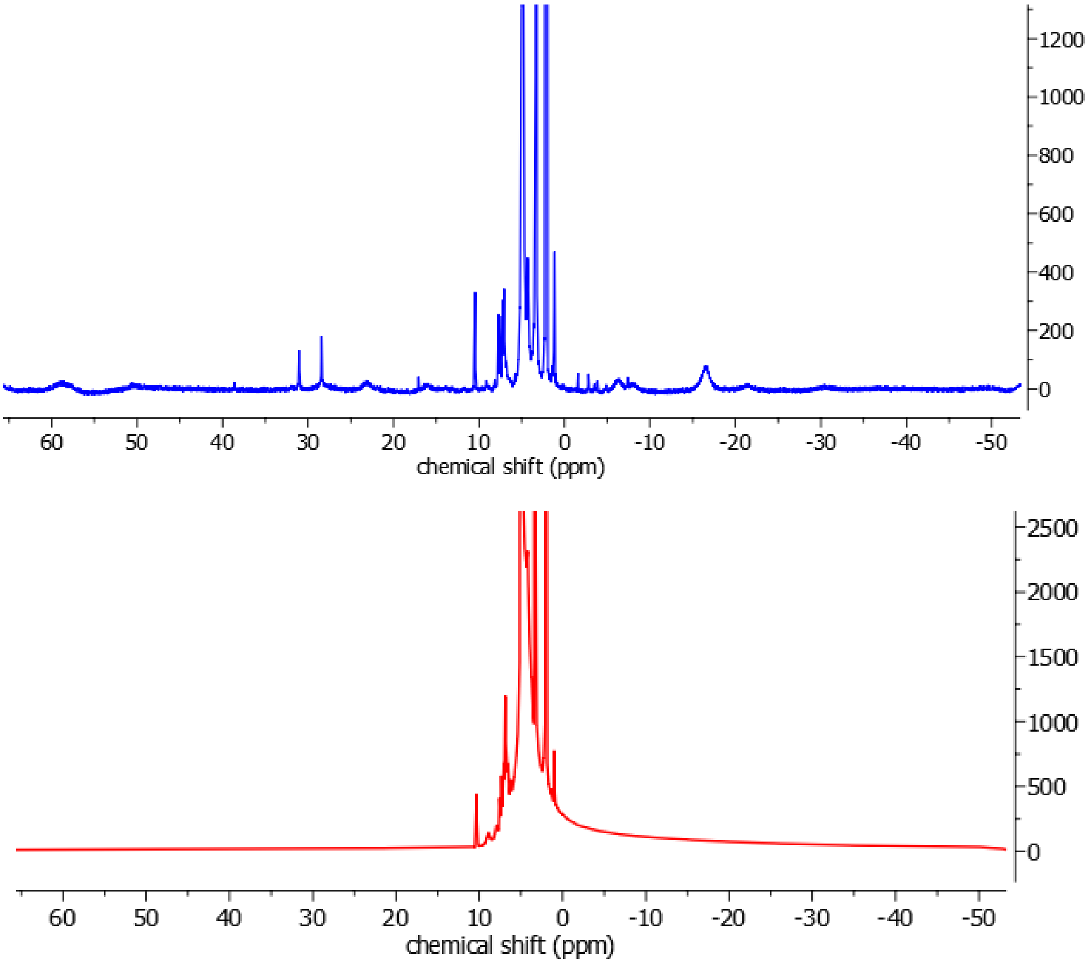

Fig. S26 Top: Paramagnetic ^{1}H-NMR spectrum of **2** in air-saturated CD_3OD. **Bottom:** ^{1}H NMR obtained of **2** in-air saturated CD_3OD after addition of 10 mM AcOH. Paramagnetic, shifted signals disappear indicating oxidative addition of O_2 to **2**, to form a dicobalt(III) species.

EPR Spectroscopy. X-band (9.4 GHz) EPR spectra of **2** in methanol solutions were obtained at room temperature on a Bruker EMX Micro X-band spectrometer, and were obtained at 10 K / 50 K using a Bruker EMX X-band spectrometer. Acquisition parameters were generally 10 scans, 20 dB attenuation and 5G modulation frequency; 30 scans were used for the air saturated samples with buffer at room temperature, to make sure no superoxo radical signal was present. The spectra are displayed with the frequency corrected to exactly 9.4 GHz in all cases. For the AcOH/TBAOAc/air system, the spectra are consistent with the NMR in showing disappearance of paramagnetism from the low temperature (10 K) spectrum, and no radical signals in the room temperature spectrum. Paramagnetism also disappears at low temperature upon addition of NH_4PF_6 and saturation with air, and no signal is observed at room temperature, or at 50 K. While this does not completely rule out short lived superoxo species, it is consistent with the proposed formation of a peroxo-bridged dicobalt(III) species in both the 4-electron (AcOH/TBAOAc) and 2-electron (NH_4PF_6) conditions.

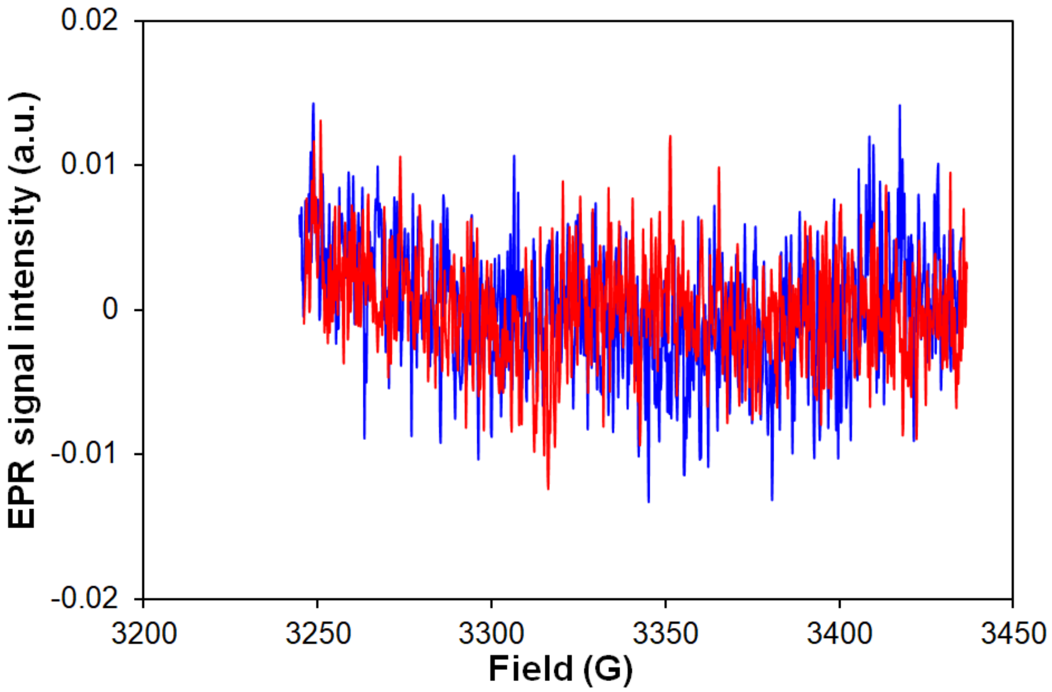

Fig. S27 Room temperature X-band EPR spectra of **2** in methanol under argon (blue) and in an air saturated methanol solution containing excess AcOH/TBAOAc (red).

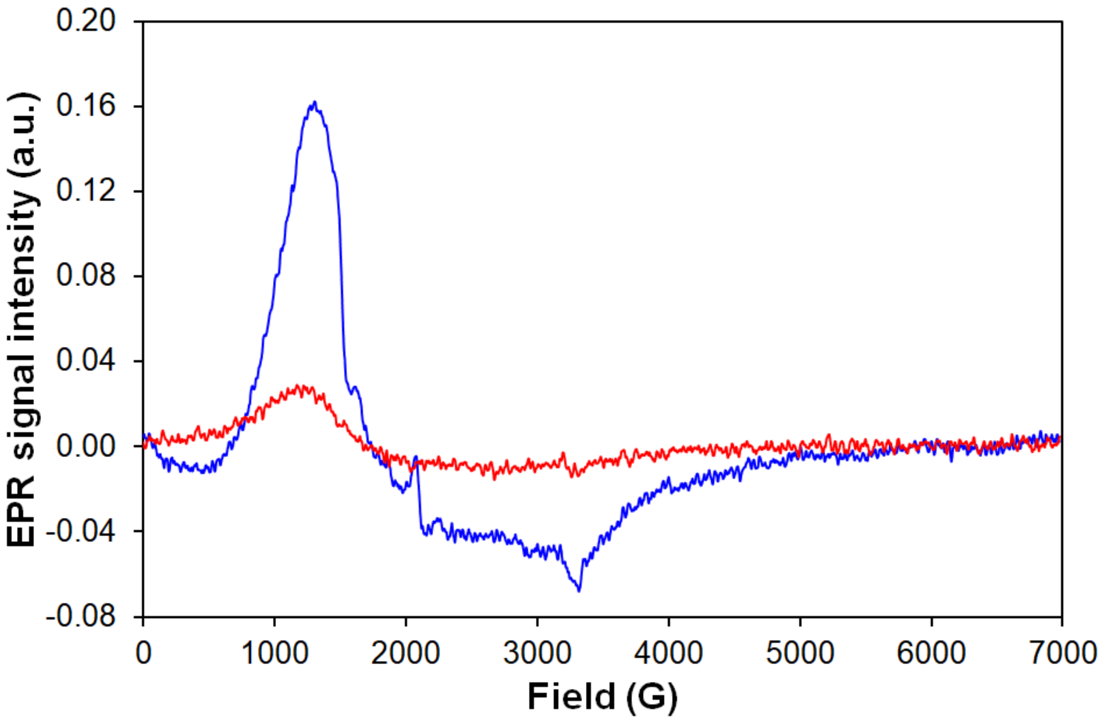

Fig. S28 Low temperature (10 K) X-band EPR spectra of **2** in methanol under argon (blue) and in an air saturated methanol solution containing excess AcOH/TBAOAc (red).

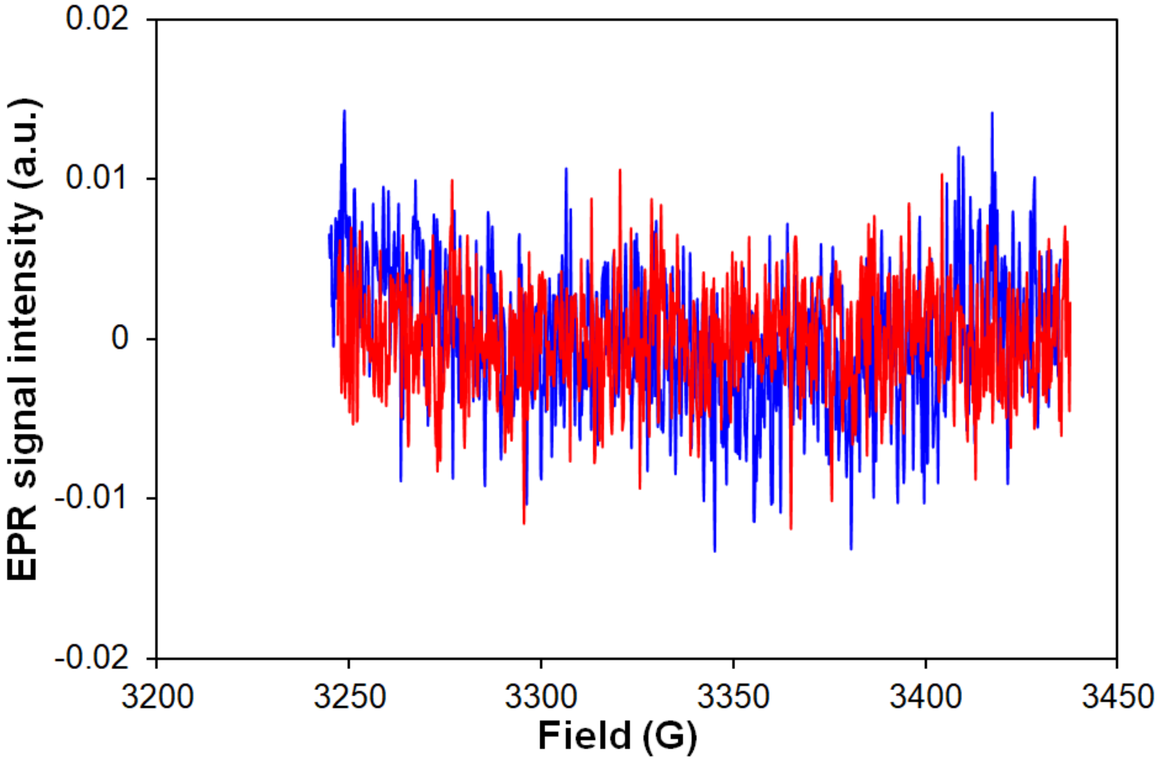

Fig. S29 Room temperature X-band EPR spectra of **2** in methanol under argon (blue) and in an air saturated methanol solution containing excess NH_4PF_6 (red).

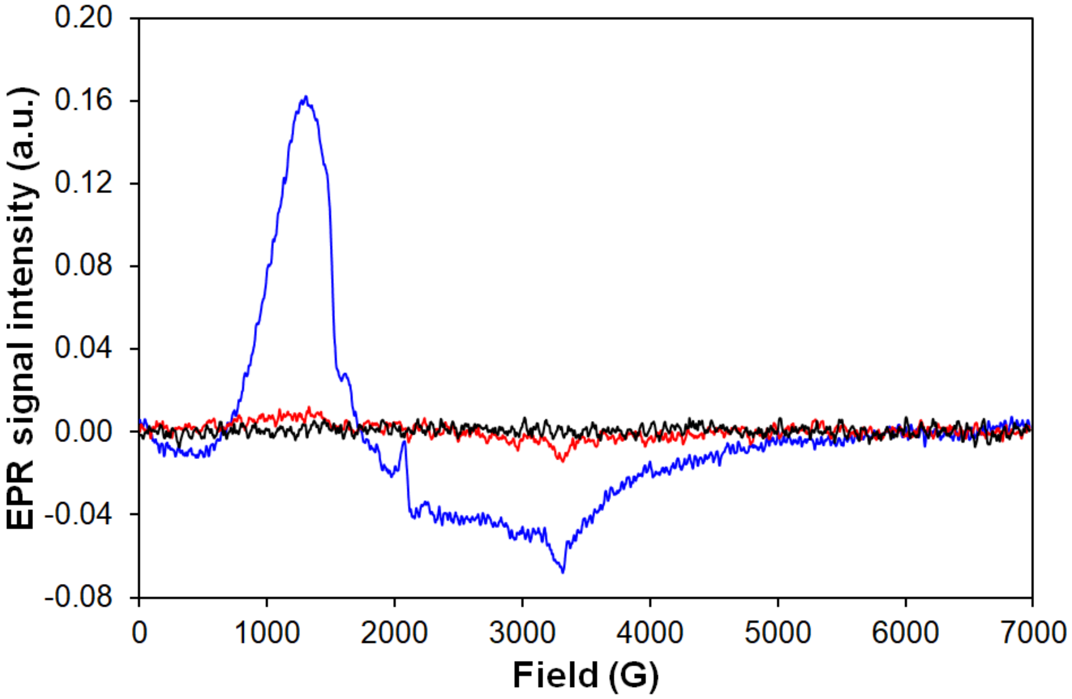

Fig. S30 Low temperature X-band EPR spectra: **2** in methanol under argon at 10 K (blue), in an air saturated methanol solution containing NH_4PF_6 at 10 K (red), and in an air saturated methanol solution containing excess NH_4PF_6 at 50 K (black).

References

1. *CrysAlisPro* (Version 1.171.40.68a), Rigaku Oxford Diffraction, Rigaku Corporation, Tokyo, Japan, 2019.

2. G. M. Sheldrick, *Acta Cryst. A*, 2015, **71**, 3.

3. O. V. Dolomanov, L. J. Bourhis, R. J. Gildea, J. A. K. Howard and H. Puschmann, *J. Appl. Crysallogr.* 2009, **42**, 339.

4. G. M. Sheldrick, *Acta. Cryst. C*, 2015, **71**, 3.

5. A. L. Spek, *Acta. Cryst. C*, 2015, **71**, 9.

6. Z. Kónya, J. Kass, A. Oszkó, A. Siska and I. Kiricsi, *Phys. Chem. Chem. Phys.* 2001, **3**, 155.

7. M. Biesinger, B. P. Payne, A. P. Grosvenor, L. W. M. Lau, A. R. Gerson and R. St.C. Smart, *Appl. Surf. Sci.* 2011, **257**, 2717.

8. J.-G. Kim, D. L. Pugmire, D. Battaghlia and M. A. Langell, *Appl. Surf. Sci.* 2000, **165**, 70.

9. (a) S. Fukuzumi, K. Okamoto, C. P. Gros and R. Guilard, *J. Am. Chem. Soc.* 2004, **126**, 10441. (b) A. M. J. Devoille and J. B. Love, *Dalton Trans.* 2011, **41**, 65. (c) Y. H. Wang, M. L. Pegis, J. M. Mayer and S. S. Stahl, *J. Am. Chem. Soc.*, 2017, **139**, 16458. (d) M. L. Pegis, D. J. Martin, C. F. Wise, A. C. Brezny, S. I. Johnson, L. E. Johnson, N. Kumar, S. Raugei and J. M. Mayer, *J. Am. Chem. Soc.* 2019, **141**, 8315.

10. Y. H. Wang, P. E. Schneider, Z. K. Goldsmith, B. Mondal, S. Hammes-Schiffer and S. S. Stahl, *ACS Cent. Sci.*, 2019, **5**, 1024.